Article

The International Journal of Robotics Research
1–26

Reprints and permissions:
sagepub.co.uk/journalsPermissions.nav
DOI: 10.1177/0278364917746222
journals.sagepub.com/home/ijr

Complete follow-the-leader kinematics using concentric tube robots

Arnau Garriga-Casanovas[1,2] and Ferdinando Rodriguez y Baena[1]

Abstract

Concentric tube robots offer the capability of follow-the-leader motion, which is desirable when navigating in cluttered environments, such as in minimally invasive surgery or in-situ inspections. The follow-the-leader capabilities identified in the existing literature, however, are limited to trajectories with piecewise constant-curvature segments or piecewise helical segments. A complete study of follow-the-leader kinematics is, therefore, relevant to determine the full potential of these robots, and clarify an open question. In this paper, a general analysis of follow-the-leader motion is presented, and a closed-form solution to the complete set of trajectories where follow-the-leader is possible under the assumption of no axial torsion of the tubes composing the robot is derived. For designs with constant-stiffness tubes, the precurvatures required are found to be either circumference arcs, helices, or deformed helices with exponentially varying curvature magnitude. The analysis developed also elucidates additional motions of interest, such as the combination of follow-the-leader motion in a robot segment with general maneuvers in another part. To determine the applicability of the assumption regarding the tubes' torsion, the general equilibrium of the robot designs of interest is considered, and a closed-form solution to torsion in two-tube robots with helical precurvatures is derived. Criteria to select a desired torsional behavior are then extracted. This enables one to identify stable trajectories where follow-the-leader is possible, for potential application to minimally invasive surgery. An illustrative case study involving simulation and experiment is conceived using one of these trajectories, and the results are reported, showcasing the research.

Keywords

Concentric tube robots, kinematics, follow-the-leader

1. Introduction

Concentric tube robots were originally proposed a decade ago by Sears and Dupont (2006) and Webster et al. (2006), and since then their popularity has been increasing, predominantly in the field of minimally invasive surgery. The rapid uptake of these robots can be credited to the advantages they offer when operating in confined environments. These advantages include a small diameter similar to that of a surgical needle, a simple mechanical design requiring a small number of parts, and singular kinematics that provide the ability to advance in follow-the-leader motion, i.e. the robot structure follows the path selected by its distal end, in specific trajectories.

A concentric tube robot consists of a set of precurved, super-elastic tubes arranged concentrically. The geometry of the robot is therefore determined by the elastic equilibrium of the tubes that compose it. The control of the relative insertion and rotation of the tubes enables control of the robot's motion. It should be noted, however, that the motion achievable by a specific robot depends on its design in terms of the precurvature and stiffness of the tubes that comprise it.

Research on the different aspects of concentric tube robots is reported in the literature. The mechanical analysis of these robots is well established, with traditional approaches assuming no external loads and no friction, such as in Dupont et al. (2009) and Webster et al. (2009), and subsequent studies considering external forces, as in Mahvash and Dupont (2011) and Rucker et al. (2010), and also including friction between tubes (Lock and Dupont, 2011). As a result, accurate control of the robots is possible (Dupont et al., 2010a,b), and stable paths can be planned (Bergeles and Dupont, 2013; Lyons et al., 2009, 2010).

[1]Mechatronics in Medicine Laboratory, Imperial College London, UK
[2]Rolls-Royce plc, UK

Corresponding author:
Arnau Garriga-Casanovas, Mechatronics in Medicine Laboratory, Department of Mechanical Engineering, Imperial College London, Exhibition Road, London, SW7 2AZ, UK.
Email: a.garriga-casanovas14@imperial.ac.uk

In addition, feedback systems based on fiber Bragg gratings have been proposed and incorporated into the robots (Ryu and Dupont, 2014), enabling closed-loop control with proprioceptive sensing.

All this established research has allowed applications in a range of medical procedures, including Burgner et al. (2011); Butler et al. (2012); Dupont et al. (2012); Gosline et al. (2012); Vasilyev et al. (2013), which showcase the capabilities of concentric tube robots. Current work, however, is focused on the exploitation of robot designs composed of piecewise constant-curvature tubes. A first study of other trajectories traceable in a follow-the-leader configuration was recently published by Gilbert et al. (2015). However, this work only offers solutions for some specific robot configurations, but it does not allow a general study, leaving general follow-the-leader possibilities as an open question. A general study is therefore required to determine the complete follow-the-leader possibilities that concentric tube robots can offer, based on existing models, thereby establishing the full potential of these devices.

In this paper, the full follow-the-leader capabilities achievable with concentric tube robots are analyzed, and a closed-form solution to the complete set of trajectories that can be followed in a follow-the-leader configuration under the assumption of no axial torsion of the tubes is presented. The validity of such an assumption is subsequently considered in the set of trajectories discovered, which allows for the selection of a case study to showcase the work. The objective of this work is similar to that in Gilbert et al. (2015), and therefore some parallels are present, as noted throughout this paper. However, the research presented here was conducted independently of Gilbert et al. (2015), which favored the formulation of a different approach that enables a general study and solution. This clarifies a currently open question, and broadens the potential of concentric tube robots with a new set of trajectories that can be exploited in, for instance, minimally invasive surgery or in-situ inspections. A crucial part of the approach adopted here is a specific robot description, which allows a geometrical interpretation of the conditions for follow-the-leader motion. This enables the formulation of a treatable problem and the derivation of a general, closed-form solution under the assumption of no axial torsion of the tubes.

The formulation of the analysis presented in this work considers robots comprising any number of tubes with any desired precurvature and stiffness, and any possible control strategy in terms of rotation and insertion of the tubes. Discontinuities in robot curvature, which are inherent in telescopic robot deployment as well as in unconventional robot designs, are also considered in the study. Thus, the analysis of follow-the-leader motion reported here, together with the corresponding solutions, is completely general. In addition, the geometrical interpretation of follow-the-leader motion proposed in this paper provides conceptual insight into these kinematics, which is useful for the future development of path planning and closed-loop control algorithms, and for the application of these robots to practical scenarios, where disturbances are present.

The strategy employed in this work to study the follow-the-leader possibilities, which involves first studying the problem assuming no torsion and then determining the validity of the assumption, is advantageous from both a theoretical and practical perspective. It establishes the full capabilities first under the assumption of no torsion, and then it enables selection of the admissible deviation in terms of torsion of the tubes. In this manner, useful trajectories with a small deviation away from an ideal follow-the-leader configuration are not discarded, which can be advantageous. Furthermore, since the admissible deviation in terms of torsion can be selected, it can be specified to be as close to zero as desired. Still, the design of concentric tube robots accepting a relatively small deviation from follow-the-leader due to torsion is advisable, considering that it noticeably increases the number of feasible trajectories, and that, in practice, a certain degree of uncertainty generally exists in the predicted robot behavior. It should be noted that the focus here is on the deviation in terms of local curvature from that corresponding to follow-the-leader motion, but this does not directly imply a specific deviation in task space. The relation between deviation in task space and local deviation due to torsion is illustrated with some simulations of relevant configurations, but the determination of the specific relation is a question beyond the scope of this present work. Interestingly, the analysis assuming no torsion is also applicable to robot designs with non-annular cross-sections, originally proposed in Greenblatt et al. (2011), by simply considering controls without relative rotation of the tubes.

To study the torsion of tubes and then conceive a case study to showcase this research, the general equilibrium of the robot is considered in the set of trajectories discovered. A closed-form solution describing the torsion of the tubes along the arc length is obtained for two-tube robots with helical precurvatures, which represent the most relevant designs in the trajectories discovered. This solution then allows for identification of the designs that guarantee that the torsion of the tubes is below a specified value. Interestingly, the torsional behavior is found to depend on two non-dimensional groups, which indicate that torsional deviation can be reduced by using helical tubes the precurvatures of which have significantly different geometric torsion. These results are used to develop a case study involving simulation and experiment, where the tubes present a small torsional deformation and the robot maintains a near perfect follow-the-leader configuration, illustrating the capabilities described in this work.

The set of trajectories found in this work is non-trivial, and expands the currently known capabilities of concentric tube robots. For robots composed of constant-stiffness tubes, the corresponding robot designs required are found

to be composed of tubes with precurvatures that are either helices or deformed helices with exponentially varying curvature magnitude. For robots with variable stiffness tubes, robot designs composed of tubes with more general geometries associated with the deformation of helices are found to be possible. It should be noted that the idea of considering helical precurvatures for follow-the-leader motion has been previously proposed by Gilbert et al. (2015), but in this work it is extended and formalized. Kinematic equivalences that can be exploited within the follow-the-leader set of trajectories are also extracted from the analysis. These include concatenation of segments of different trajectories, or the addition of idle tubes that become active once inserted. Furthermore, various maneuvers that combine follow-the-leader motion along a segment of the concentric tube robot with general displacements at its distal end, which do not correspond to follow-the-leader, are also distilled from the analysis. These maneuvers are aimed at applications where the robot end-effector is able work in a spacious cavity, which can only be accessed through a narrow path that requires follow-the-leader motion. Such a situation is common in minimally invasive surgery, as well as in other fields, such as in-situ inspections, where the kinematics identified here can offer a significant advantage. It should be noted that the majority of these kinematic possibilities have already been proposed in the literature for robot designs composed of piecewise constant-curvature tubes (e.g. Dupont et al., 2010b, 2012; Gosline et al., 2012). In this work, these are generalized and integrated into the analysis developed here.

The paper is structured as follows. The governing equations of a general concentric tube robot under the assumption of no axial torsion are derived in Section 2. The study of follow-the-leader motion is presented Section 3, where the closed-form solution corresponding to the trajectories traceable in a follow-the-leader configuration is derived. In Section 4, additional maneuvers of interest that can be deduced from the analysis of follow-the-leader motion are described. The structural analysis considering torsion of the tubes composing a robot is outlined in Section 5, including the closed-form solution to the tubes' torsion in a two-tube configuration. Finally, the case study involving simulation and experiment is presented in Section 6, together with the corresponding results, which leads to the conclusion of the paper in Section 7.

2. Governing equations

The relations that govern the behavior of the robotic system are derived in this section. The analysis follows a similar approach to that in the established literature, and Dupont et al. (2010b) is used as the main reference throughout the paper to facilitate the reading. However, some variations on the analysis are introduced in order to adapt it to the aims of this work, with associated changes in nomenclature.

2.1. Problem characterization

The problem description adopted in this work is crucial to enable derivation of the solutions presented in the following sections. In this regard, a detailed characterization of the problem is presented in this subsection. The geometry of a tube, or a set of concentric tubes, is described by the curve corresponding to its centerline. Diameter variations are not expected, nor relevant to this study, and only the cross-sectional moment of inertia is necessary, as elucidated in the following subsection. Vectors, and in particular curvature, are expressed using Bishop reference frames (Bishop, 1975). In particular, a frame W is defined as a Bishop frame corresponding to the final robot geometry, as initially proposed by Sears and Dupont (2006), and a frame F_i is defined as a frame materially attached to a tube i that coincides with a Bishop frame associated with tube i before undergoing structural deformation.

The following magnitudes are then used to characterize a concentric tube robot. The length of the relevant part of the robot, which generally corresponds to the inserted robot length, is denoted L. The position along the arc length is represented by s, relative to the distal end and defined positive $s \in [0, L]$. An independent variable t, generally coinciding with time, is used to parametrize the evolution of the robotic system. The vector curvature of tube i at cross-section s_i and instant t is denoted by the first two components of $\mathbf{u}_i^{F_i(s_i)}(s_i, t) = [u_{ix}, u_{iy}, u_{iz}]^{\mathrm{T}}$, which is defined as the angular rate of increment of frame F_i materially attached to tube i with respect to the arc length, and expressed in the same frame $F_i(s_i)$. The third component of $\mathbf{u}_i^{F_i(s_i)}(s_i, t)$ denotes the torsional deformation of tube i. Similarly, the first two components of $\mathbf{u}_T^{W(s)}(s, t)$ define the curvature of the resulting robot in frame $W(s)$, while the third component of $\mathbf{u}_T^{W(s)}(s, t)$ is zero, owing to the definition of W. It should be noted that the vector curvature of a tube before and after applying external wrenches on it generally varies, so a circumflex is used to indicate the initial curvature $\hat{\mathbf{u}}_i^{F_i}(s_i)$. Since the initial geometry of a tube is described by the curve corresponding to its centerline, expressed in a Bishop frame, the third component of the initial curvature is zero, by definition $\hat{u}_{iz}^{F_i}(s_i) = 0$. The stiffness matrix corresponding to a tube i is defined as

$$\mathbf{k}_i = \begin{bmatrix} E_{ix}I_{ix} & 0 & 0 \\ 0 & E_{iy}I_{iy} & 0 \\ 0 & 0 & J_iG_i \end{bmatrix}$$

where E is the Young modulus and $I_{ix,y}$ is the cross-sectional moment of inertia in either direction x or y. In this work, the tubes are assumed to have an annular cross-section, since this allows relative rotation between the tubes, and it is therefore the most general case in terms of follow-the-leader motion analysis. This implies $E_{ix}I_{ix} = E_{iy}I_{iy}$; therefore, the matrix $\mathbf{k}_i$ is independent of the Bishop frame used in the tube or robot description. The length along the robot centerline between the distal end of tube i and the robot's

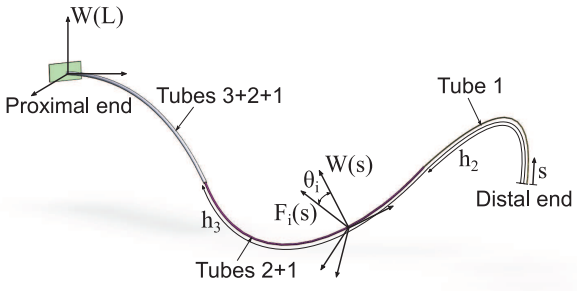

Fig. 1. General concentric tube robot composed of three tubes with relevant nomenclature definitions.

distal end is defined as h_i. At least one h_i must be zero, since the robot's distal end must comprise at least one tube, and here h_1 is chosen to be zero in a situation of ambiguity. The rotation angle between frame F_i and frame W is denoted by θ_i. The scalar velocity at which the distal end of the robot advances through the workspace with respect to t is represented by v. Finally, the internal moment vector associated with the resulting cross-sectional stress of tube i is indicated as $\mathbf{m}_i^{F_i}$. A general concentric tube robot with some of the magnitudes defined defined is illustrated in Figure 1.

From this problem description, the advantages of using Bishop frames (Bishop, 1975) are clear. First, Bishop frames are intrinsic reference frames with one component always parallel to the curve tangent vector, which is convenient, considering that the vector curvature is orthogonal to the tube's centerline curve. In addition, they are defined in any curve that is sufficiently differentiable, even at points with zero curvature. Finally, for a tube with no axial torsion, the curvature along the tube can be transformed to another Bishop frame with a simple rotation that is constant along the entire tube.

2.2. Governing laws

The behavior of the robotic system is governed by three laws. First, an elastic constitutive law, which can be obtained following Dupont et al. (2010b) as

$$\mathbf{m}_i^{F_i} = \mathbf{k}_i \left(\mathbf{u}_i^{F_i} - \hat{\mathbf{u}}_i^{F_i} \right) \tag{1}$$

Second, a static equilibrium law (assuming a quasistatic operation of the robot), which can be written as

$$\sum_{i=1}^{n} \mathbf{m}_i^{W(s)} = 0 \tag{2}$$

Finally, a law preventing the superposition of matter (using a continuum mechanics description of matter), which translates into a condition that imposes a common final curvature to the tubes that compose a robot when arranged concentrically

$$\mathbf{u}_1^{W(s)}|_{x,y} = \mathbf{u}_2^{W(s)}|_{x,y} = \ldots = \mathbf{u}_T^{W(s)}|_{x,y} \tag{3}$$

which only applies to the x, y components of $\mathbf{u}_i^{W(s)}$, as indicated by the subscripts x, y.

Assuming no external loads, and no axial torsion of the tubes, combination of all three laws (equations (1), (2), and (3)) determines the robot quasistatic model

$$\mathbf{u}_T^{W(s)}(s,t) = \left[\sum_{j=1}^{n} \mathbf{k}_j \right]^{-1} \sum_{i=1}^{n} \mathbf{R}(\theta_i(t))\, \mathbf{k}_i \hat{\mathbf{u}}_i^{F_i}(s - h_i(t)) \tag{4}$$

where $h_1 = 0$, n is the number of tubes comprising the robot, and

$$\mathbf{R}(\theta_i(t)) = \begin{bmatrix} \cos(\theta_i(t)) & -\sin(\theta_i(t)) & 0 \\ \sin(\theta_i(t)) & \cos(\theta_i(t)) & 0 \\ 0 & 0 & 1 \end{bmatrix}$$

expressed in a Bishop frame corresponding to the final robot curvature with no axial torsion. The orientation of this final Bishop frame around the z axis is defined by a desired arbitrary frame in a given cross-section, e.g. the proximal end of the robot, and the corresponding extension to the entire curve of the robot centerline. As a consequence, rigid body rotations of the robot are represented by a simple rotation of all tubes with a common angular velocity. It should be noted that the composition $(s - h_i(t))$ allows the evaluation of each tube's stiffness and initial curvature in a given cross-section relative to the robot reference frame.

Equation (4) elucidates the fact that both the tubes and the robot's final curvature can be expressed using a vector with only two components. However, in order to be consistent with literature, and to clarify the use of the assumption of no axial torsion, a three-dimensional vector is employed.

3. Follow-the-leader

Equation (4) describes all possible geometries that a concentric tube robot with design parameters $\mathbf{k}_i, \hat{\mathbf{u}}_i$ can achieve by relative rotation and insertion of the tubes that integrate it, and, therefore, the general movements it can perform. At each cross-section, the possible robot curvature evolutions with time are given by the functions $\theta_i(t)$ and $h_i(t)$ for all tubes. And for a given instant in time, the shape of the continuum robot is determined by the curvature values along s.

In this section, the robot kinematics corresponding to follow-the-leader motion are studied. The condition for follow-the-leader motion is first elucidated in Subsection 3.1. This condition is then imposed on the quasistatic model of a general concentric tube robot in Subsection 3.2, yielding the vectorial equation that must be satisfied for a trajectory to be traceable in follow-the-leader motion. The complete solutions to this equation are then studied in Subsection 3.3, leading to the complete set of trajectories where follow-the-leader is possible in Subsection 3.4. It should be noted that the strategy of defining a kinematic condition for follow-the-leader motion and then imposing it on the robot

model is similar to that proposed in Gilbert et al. (2015). However, the specific analysis is markedly different, which is a consequence of the fact that this research was conducted independently. In this regard, the study in this paper is complementary to that of Gilbert et al. (2015), and in this case leads to the solutions derived in the following subsections.

3.1. General condition

Follow-the-leader motion requires the curve corresponding to the robot centerline to remain in a constant spatial curve, except for the differential segment that advances with a differential of t. Thus, the curvature of the robot centerline must be constant for all spatial locations. Defining a magnitude x, which corresponds to spatial location in the workspace, the condition imposing curvature at each spatial location to remain constant can be expressed as

$$\mathbf{u}_T(x) = \text{constant} \qquad \forall x \in C \tag{5}$$

where C is the locus of the curve corresponding to the robot centerline. Considering that the robot curvature can be expressed as a function of s and t, as described in the previous section, the expression of curvature at a spatial location can be differentiated. Since the curvature must be constant at each spatial location, as expressed in equation (5), differentiation yields the condition for follow-the-leader in the robot segments with differentiable curvature as

$$-v\frac{\partial \mathbf{u}_T^{W(s)}}{\partial s} = \frac{\partial \mathbf{u}_T^{W(s)}}{\partial t} \qquad \forall s, t \tag{6}$$

It should be noted that the time-dependent variables in $\mathbf{u}_T^{W(s)}$ are $\theta_i(t)$ and $h_i(t)$, and therefore the right hand side of equation (6) corresponds to

$$\frac{\partial \mathbf{u}_T^{W(s)}}{\partial \theta_i, h_i \ldots}\frac{\partial \theta_i, h_i \ldots}{\partial t}$$

for all i. Equation (6) indicates that, in order to advance in a follow-the-leader configuration, the curvature of each cross-section must pass to the immediate adjacent cross-section toward the proximal end. In a reference frame positioned at the distal end of the robot, this motion resembles that of a wave without attenuation traveling toward the base of the concentric tube robot, as conceptually illustrated in Figure 2.

For robots with continuous $\partial \mathbf{u}_T^{W(s)}/\partial s$ and $\partial \mathbf{u}_T^{W(s)}/\partial t$, equation (6) is a necessary and sufficient condition for follow-the-leader motion. For robots with discontinuities in $\nabla \mathbf{u}_T^{W(s)}$, follow-the-leader motion is achieved if and only if the discontinuity step is finite, constant, and translating at velocity v away from the distal end, and also equation (6) is satisfied in the segments of continuity. In other words, follow-the-leader requires the curvature discontinuity to remain constant in the given position relative to the workspace, and therefore it must translate away at rate v from the robot distal end as the robot advances.

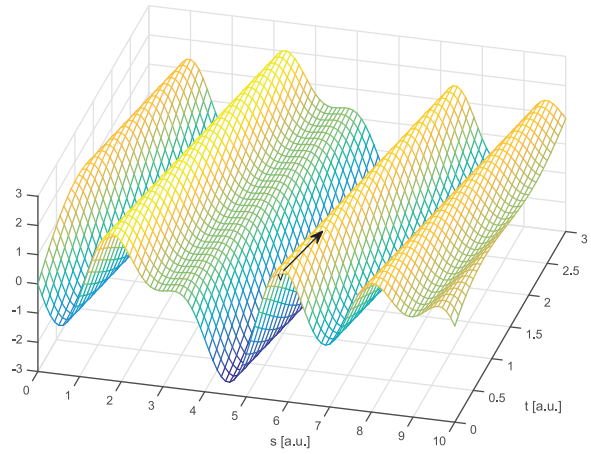

Fig. 2. Conceptual illustration of a Curvature field corresponding to follow-the-leader configuration. A vector of motion that satisfies follow-the-leader is indicated with a black arrow.

3.2. Application to concentric tube robots

The imposition of equation (6) on the quasistatic model of the robot (equation (4)) restricts the possible robot kinematics to those that correspond to perfect follow-the-leader motion (if any). This yields the condition that suffices for a trajectory to be traceable by a concentric tube robot in a follow-the-leader configuration

$$\sum_{i=1}^{n}\left[\mathbf{R}'(\theta_i)\,\mathbf{P}_i\hat{\mathbf{u}}_i^{F_i}(s-h_i)\,\dot{\theta}_i - \mathbf{R}(\theta_i)\,\frac{\partial}{\partial s}(\,\mathbf{P}_i\hat{\mathbf{u}}_i^{F_i}(s-h_i)\,)\,\dot{h}_i\right] = -v\sum_{i=1}^{n}\left[\mathbf{R}(\theta_i)\,\frac{\partial}{\partial s}\left(\mathbf{P}_i\hat{\mathbf{u}}_i^{F_i}(s-h_i)\right)\right] \qquad \forall s, t \tag{7}$$

where

$$\mathbf{R}'(\theta_i(t)) = \begin{bmatrix} -\sin(\theta_i(t)) & -\cos(\theta_i(t)) & 0 \\ \cos(\theta_i(t)) & -\sin(\theta_i(t)) & 0 \\ 0 & 0 & 0 \end{bmatrix}$$

and

$$\mathbf{P}_i = \left[\sum_{j=1}^{n}\mathbf{k}_j\right]^{-1}\mathbf{k}_i$$

and both $\dot{\theta}_i$ and $\dot{h}_i$ are functions of time. The dependence of $\dot{\theta}_i$ and $\dot{h}_i$ on t is omitted in equation (7) and in the following equations for brevity, but both $\dot{\theta}_i$ and $\dot{h}_i$ should be considered to be functions of time in the entire presentation unless otherwise stated.

The curve describing trajectories where follow-the-leader is possible can be specified both by the corresponding $\mathbf{u}_T^W(s, t_\mathrm{f})$, which is parametrized by the arc length and evaluated at the time at the end of an insertion t_f, or by $\mathbf{u}_T^W(0, t)$, which is parametrized by time and evaluated at the robot distal end $s = 0$. Both expressions are equivalent in a follow-the-leader configuration. In this presentation, the expression $\mathbf{u}_T^W(s, t_\mathrm{f})$ is used for clarity of exposition.

In concentric tube robots, $\partial \mathbf{u}_T^{W(s)}/\partial s$ and $\partial \mathbf{u}_T^{W(s)}/\partial t$ must be sectionally continuous since discontinuities can only be caused by either the end of one tube, or a locally non-differentiable precurvature, both of which generate constant discontinuity steps. In this regard, the translation of discontinuity points toward the robot's proximal end at velocity v, and satisfaction of equation (7) in the rest of the domain, are necessary and sufficient conditions for a trajectory to be traceable in a follow-the-leader configuration.

The complete solution to equation (7) therefore corresponds to the complete set of trajectories where follow-the-leader is possible under the assumption of no axial torsion. It should be noted that equation (7) is applicable to any robot design in terms of precurvatures, stiffness, and number of tubes, for any possible control strategy. Thus, it represents a general condition for follow-the-leader motion.

The problem description employed in this work allows the derivation of a closed-form solution to equation (7). The key to such a solution is to treat equation (7) from a vectorial perspective, rather than decoupling it into a system of individual differential equations. Considering that all terms in equation (7) either contain $\mathbf{P}_i\hat{\mathbf{u}}_i^{F_i}$ or its derivative relative to s, and that $\mathbf{R}$ and $\mathbf{R}'$ are closely related in terms of the rotations they represent, geometric relations simplify the study of equation (7). Such geometric interpretation also provides insight into the control inputs and geometries associated with follow-the-leader motion, and facilitates an intuitive interpretation of the follow-the-leader configuration. The rest of this section is dedicated to the solution of equation (7).

3.3. Solution cases

The approach adopted here to study the solution to equation (7) involves dividing the problem into cases of increasing complexity for clarity of exposition, as presented in this subsection. Cases with restrictions on the motions allowed with the tubes are considered first, serving as a foundation for the subsequent study of more general cases.

3.3.1. Rotation only and different for each tube. Considering first a case where the rotation of the tubes is the only input allowed (equal insertion rate of all tubes), and considering that no groups of tubes are moving together, i.e. functions $\dot{\theta}_i(t)$ satisfy $\dot{\theta}_i(t) \neq \dot{\theta}_j(t)\ \forall i,j = 1,\ldots,n$ over the course of an insertion, equation (7) simplifies to

$$\sum_{i=1}^{n} \mathbf{R}'(\theta_i)\,\mathbf{P}_i\hat{\mathbf{u}}_i^{F_i}(s)\,\dot{\theta}_i = -v\sum_{i=1}^{n} \mathbf{R}(\theta_i)\,\frac{\partial}{\partial s}\left(\mathbf{P}_i\hat{\mathbf{u}}_i^{F_i}(s)\right) \quad (8)$$

The possible solutions to equation (8) can be divided into two cases: the terms in equation (8) corresponding to each tube compensate so that their sum is null, which will be referred to as "compensating individually", or the terms in equation (8) from different tubes combine so that their sum is zero, which will be referred to as "compensating in conjunction."

In the case of compensating individually, equation (8) is particularized as

$$\mathbf{R}'(\theta_i)\,\mathbf{P}_i\begin{bmatrix}\hat{u}_{ix}\\ \hat{u}_{iy}\\ 0\end{bmatrix}(s)\,\dot{\theta}_i = -v\mathbf{R}(\theta_i)\,\frac{\partial}{\partial s}\left(\mathbf{P}_i\begin{bmatrix}\hat{u}_{ix}\\ \hat{u}_{iy}\\ 0\end{bmatrix}(s)\right) \quad (9)$$

which must be satisfied for all time. The only time-dependent terms are matrices $\mathbf{R}$ and $\mathbf{R}'$ and $\dot{\theta}_i(t)$. Realizing that both $\mathbf{R}$ and $\mathbf{R}'$ matrices represent a rotation of the x and y components with a constant difference of $\pi/2$, and that component z is not relevant here, since the vector curvature always lies in the XY plane, equation (9) reduces to an ordinary differential equation of the vector $\mathbf{P}_i\hat{\mathbf{u}}_i$ with respect to s

$$\mathbf{R}\left(\frac{\pi}{2}\right)\mathbf{P}_i\begin{bmatrix}\hat{u}_{ix}\\ \hat{u}_{iy}\\ 0\end{bmatrix}(s)\,\dot{\theta}_i = -v\frac{\partial}{\partial s}\left(\mathbf{P}_i\begin{bmatrix}\hat{u}_{ix}\\ \hat{u}_{iy}\\ 0\end{bmatrix}(s)\right) \quad (10)$$

The solution to equation (10) can be easily obtained by realizing that it imposes $\partial(\mathbf{P}_i\hat{\mathbf{u}}_i)/\partial s$ to be orthogonal to $\mathbf{P}_i\hat{\mathbf{u}}_i$. Specifically, the modulus $\left\|\mathbf{P}_i\hat{\mathbf{u}}_i\right\|$ must be constant, and the direction of the vector $\mathbf{P}_i\hat{\mathbf{u}}_i$ corresponding to tube i in a Bishop frame must rotate in the local XY plane at a constant rate with respect to the arc length. In addition, $\dot{\theta}_i(t)$ must be constant and proportional to v in order to satisfy equation (10) for all t. This applies to any individual tube, and therefore configurations corresponding to robots composed of individual tubes that satisfy equation (10) correspond to trajectories that satisfy follow-the-leader.

Follow-the-leader motion using only relative rotation of the tubes and compensating individually is therefore possible, and the resulting trajectories expressed as the resulting geometry of the robot at the time corresponding to the end of an insertion are

$$\mathbf{u}_T^W(s,t_f) = \sum_{i=1}^{n}\begin{bmatrix}\left\|\mathbf{P}_i\hat{\mathbf{u}}_i\right\|\cos(w_i s+\phi_i)\\ \left\|\mathbf{P}_i\hat{\mathbf{u}}_i\right\|\sin(w_i s+\phi_i)\\ 0\end{bmatrix} \quad (11)$$

where w_i is a variable that can be selected in the robot design as desired and corresponds to the initial torsion of tube i, and ϕ_i is a parameter related to the relative rotation of the tubes at the proximal end of the trajectory, which can also be chosen freely. It should be noted that the trajectories (equation (11)) are parametrized by s to elucidate that they correspond to a set of geometric curves, although the trajectories could also be parametrized by t, since both of these are equivalent in a follow-the-leader configuration.

In the case of compensating in conjunction, solutions to equation (8) can also be derived in specific configurations. Rewriting equation (8), relying on the fact that

$$\mathbf{R}'(\theta_i) = \mathbf{R}(\theta_i)\,\mathbf{R}\left(\frac{\pi}{2}\right)$$

yields

$$\sum_{i=1}^{n} \mathbf{R}(\theta_i)\left[\mathbf{R}\left(\frac{\pi}{2}\right)\mathbf{P}_i\hat{\mathbf{u}}_i^{F_i}(s)\,\dot{\theta}_i + v\frac{\partial}{\partial s}\left(\mathbf{P}_i\hat{\mathbf{u}}_i^{F_i}(s)\right)\right] = 0 \quad \forall s,t \quad (12)$$

The terms in equation (12) are a sum of planar vectors in each cross-section, and thus vectors $\mathbf{P}_i\hat{\mathbf{u}}_i^{F_i}$ and $\partial\mathbf{P}_i\hat{\mathbf{u}}_i^{F_i}/\partial s$ from a set of two or more tubes, defined as tubes $i \in l$, can be combined so that their sum is zero. For $\dot{\theta}_i(t) \neq \dot{\theta}_j(t)$, however, the relative orientation between vectors corresponding to different tubes changes with t. For follow-the-leader to be satisfied, these vectors need to compensate in conjunction at each instant of time and each cross-section so that their sum is null, despite variations in their relative orientation from different evolutions of $\mathbf{R}(\theta_i(t))$.

The magnitude of the vectors in equation (12) is either fixed, for $\partial\mathbf{P}_i\hat{\mathbf{u}}_i^{F_i}/\partial s$, or determined by $\dot{\theta}_i$, for $\dot{\theta}_i\mathbf{P}_i\hat{\mathbf{u}}_i^{F_i}$. The $\mathbf{P}_i\hat{\mathbf{u}}_i^{W}$ of tubes $i \in l$ are generally not aligned and therefore the $\dot{\theta}_i$ determine the value of the sum of vectors corresponding to tubes $i \in l$ in equation (12) in each cross-section. The $\dot{\theta}_i(t)$ can thus be selected so that the terms from a set of tubes l compensate in conjunction despite variations from different $\mathbf{R}(\theta_i(t))$, with the values of $\dot{\theta}_i(t)$ chosen at each instant of time for each arrangement of vectors $\mathbf{P}_i\hat{\mathbf{u}}_i^{F_i}$ and $\partial\mathbf{P}_i\hat{\mathbf{u}}_i^{F_i}/\partial s$. This enables a set of specific solutions, which are discussed in two further cases for clarity of exposition.

Considering first a case with $l = 2$, two variables $\dot{\theta}_1$ and $\dot{\theta}_2$ are available to be selected at each instant of time. Specific functions $\dot{\theta}_1(t)$ and $\dot{\theta}_2(t)$ can thus be used to satisfy the two scalar equations implied by equation (12) for a given cross-section, and all t. The functions $\dot{\theta}_1(t)$, $\dot{\theta}_2(t)$ to satisfy equation (12) are unique for a given set of $\mathbf{P}_1\hat{\mathbf{u}}_1^{F_1}$, $\partial\mathbf{P}_1\hat{\mathbf{u}}_1^{F_1}/\partial s$, $\mathbf{P}_2\hat{\mathbf{u}}_2^{F_2}$, $\partial\mathbf{P}_2\hat{\mathbf{u}}_2^{F_2}/\partial s$ with a specific relative orientation and relative magnitude between these vectors, corresponding to a given cross-section. The $\dot{\theta}_i(t)$, however, are common for all cross-sections. Follow-the-leader is then satisfied if and only if the arrangement of vectors $\mathbf{P}_i\hat{\mathbf{u}}_i^{W_i}$ and $\partial\mathbf{P}_i\hat{\mathbf{u}}_i^{W_i}/\partial s$, in terms of relative orientation and relative magnitude of these vectors for tubes $i \in l$, is proportional in all cross-sections along the arc length.

Two possible design solutions then arise: (i) $\mathbf{P}_i\hat{\mathbf{u}}_i^{W}$ and $\partial\mathbf{P}_i\hat{\mathbf{u}}_i^{W}/\partial s$ of tubes $i \in l$ remain proportional along the arc length with an equal orientation, or (ii) $\mathbf{P}_i\hat{\mathbf{u}}_i^{W}$ and $\partial\mathbf{P}_i\hat{\mathbf{u}}_i^{W}/\partial s$ remain proportional along the arc length, with an absolute orientation of all vectors corresponding to $i \in l$ rotating at a constant rate along the arc length when expressed in a Bishop frame. In solution (i), $\left\|\mathbf{P}_i\hat{\mathbf{u}}_i\right\|$ of each tube must vary exponentially in order to maintain proportionality between $\mathbf{P}_i\hat{\mathbf{u}}_i^{W}$ and $\partial\mathbf{P}_i\hat{\mathbf{u}}_i^{W}/\partial s$, and vector orientation must remain constant. In addition, the exponential increase rate must be equal for tubes $i \in l$ to maintain proportionality between all vectors corresponding to tubes $i \in l$. In solution (ii), $\left\|\mathbf{P}_i\hat{\mathbf{u}}_i\right\|$ must also vary exponentially at an equal rate for all tubes $i \in l$; in addition, the direction of $\mathbf{P}_i\hat{\mathbf{u}}_i^{W}$ and $\partial\mathbf{P}_i\hat{\mathbf{u}}_i^{W}/\partial s$ must rotate along the arc length at an equal rate for tubes $i \in l$ in order to maintain proportionality.

Considering a general case with $l > 2$, an equivalent analysis applies, although some specific differences are present. The number of variables $\dot{\theta}_i$ available in this case is l. This could suggest that equation (12) could be satisfied in $l/2$ different cross-sections (for even l) by selecting specific values of $\dot{\theta}_i$ at each instant of time. The design in terms of vectors $\mathbf{P}_i\hat{\mathbf{u}}_i^{W}$ and $\partial\mathbf{P}_i\hat{\mathbf{u}}_i^{W}/\partial s$ would then be freely selected at $l/2$ cross-sections, and designs with all other cross-sections proportional in terms of the $\mathbf{P}_i\hat{\mathbf{u}}_i^{W}$ and $\partial\mathbf{P}_i\hat{\mathbf{u}}_i^{W}/\partial s$ to any of the selected $l/2$ cross-sections, or linear combinations of them, would maintain follow-the-leader with the same common $\dot{\theta}_i$, as in the previous case for $l = 2$. However, designs with vectors $\mathbf{P}_i\hat{\mathbf{u}}_i^{W}$ and $\partial\mathbf{P}_i\hat{\mathbf{u}}_i^{W}/\partial s$ proportional to the arrangement of these vectors in multiple cross-sections are not possible. As described for the case $l = 2$, proportionality in $\mathbf{P}_i\hat{\mathbf{u}}_i^{W}$ and $\partial\mathbf{P}_i\hat{\mathbf{u}}_i^{W}/\partial s$ implies an exponential variation in $\left\|\mathbf{P}_i\hat{\mathbf{u}}_i\right\|$. Thus, proportionality of vectors $\mathbf{P}_i\hat{\mathbf{u}}_i^{W}$ and $\partial\mathbf{P}_i\hat{\mathbf{u}}_i^{W}/\partial s$ for tubes $i \in l$ to any given cross-section is propagated over all cross-sections, and consequently all cross-sections must be proportional to any given one. Therefore, also in the case $l > 2$, the arrangement of $\mathbf{P}_i\hat{\mathbf{u}}_i^{W}$ and $\partial\mathbf{P}_i\hat{\mathbf{u}}_i^{W}/\partial s$ for tubes $i \in l$ in all cross-sections must be proportional to a given cross-section for follow-the-leader compensating in conjunction to be possible. The design of the tubes is then equivalent to that in the case $l = 2$, with $\mathbf{P}_i\hat{\mathbf{u}}_i^{W}$ and $\partial\mathbf{P}_i\hat{\mathbf{u}}_i^{W}/\partial s$ for tubes $i \in l$ that must remain proportional along the arc length in terms of relative orientation and magnitude, and with an absolute orientation that must either be equal in all cross-sections, or rotating at a constant rate along the arc length.

The trajectories that can be traced in a follow-the-leader configuration with robots comprising only a set of tubes $i \in l$ that compensate in conjunction must then correspond to a $\mathbf{u}_T^{W}(s,t_\mathrm{f})$ of either constant direction or constantly rotating direction, and magnitude varying exponentially. These trajectories are

$$\mathbf{u}_T^{W}(s,t_\mathrm{f}) = \sum_{i=1}^{l}\begin{bmatrix} e^{\lambda s}\left\|\mathbf{P}_i\hat{\mathbf{u}}_i\right\|\cos(\rho s+\phi_i) \\ e^{\lambda s}\left\|\mathbf{P}_i\hat{\mathbf{u}}_i\right\|\sin(\rho s+\phi_i) \\ 0 \end{bmatrix} \quad (13)$$

where λ is a parameter corresponding to the increase in curvature magnitude along the arc length, which can be selected with the tubes' design and is common for tubes $i \in l$, ρ is a parameter corresponding to the geometric torsion of the tubes, also common for tubes $i \in l$, and ϕ_i is related to the tubes' orientation at the proximal end, as previously defined. Since ρ and λ are common for tubes $i \in l$, the trajectories (equation (13)) can also be expressed as

$$\mathbf{u}_T^{W}(s,t_\mathrm{f}) = \begin{bmatrix} e^{\lambda s}\left\|\mathbf{u}_R\right\|\cos(\rho s+\nu) \\ e^{\lambda s}\left\|\mathbf{u}_R\right\|\sin(\rho s+\nu) \\ 0 \end{bmatrix} \quad (14)$$

where $\|\mathbf{u}_R\|$ is the curvature resulting from the interaction of tubes $i \in l$ at a given cross-section, $s = 0$, and t_f, and ν

is related to the robot orientation at the proximal end, and is analogous to ϕ_i.

Compensating in conjunction requires at least two tubes in order to have two inputs $\dot{\theta}_i$ to satisfy the two components of equation (12). Configurations with additional tubes are also possible, and in these cases a degree of freedom appears for each additional tube. This does not expand the set of trajectories (equation (14)), but implies that a $\theta_i(t)$ can generally be freely selected for each additional tube, which can be exploited in additional maneuvers, described in Section 4.

Follow-the-leader motion using only relative rotation of the tubes is thus possible both compensating individually and in conjunction. Equation (8) is a summation of terms corresponding to different tubes. Hence, any combination of solutions corresponding to a set of tubes compensating individually (equation (11)) and a set of tubes compensating in conjunction (equation (14)) must also satisfy equation (8). The resulting set of trajectories is then

$$\mathbf{u}_T^W(s,t_f) = \sum_{i=1}^{n'} \begin{bmatrix} \left\|\mathbf{P}_i\hat{\mathbf{u}}_i\right\| \cos(w_i s+\phi_i) \\ \left\|\mathbf{P}_i\hat{\mathbf{u}}_i\right\| \sin(w_i s+\phi_i) \\ 0 \end{bmatrix} + \sum_{j=1}^{g} \begin{bmatrix} e^{\lambda_j s}\left\|\mathbf{u}_{R,j}\right\| \cos(\rho_j s+\nu_j) \\ e^{\lambda_j s}\left\|\mathbf{u}_{R,j}\right\| \sin(\rho_j s+\nu_j) \\ 0 \end{bmatrix} \quad (15)$$

where g is the number of sets of tubes that involve compensating in conjunction, and n' is the number of tubes that compensate individually.

As a particular solution to equation (15), the trajectory corresponding to a single tube being inserted is a helix relative to the workspace. In this case, the required tube precurvature is equal to the resulting trajectory, a configuration that corresponds to a common device, namely the corkscrew. It should be noted that the helix can be degenerated to a circumference arc, elucidating the fact that this result is completely general.

3.3.2. Different rotation and insertion for each tube. Considering now the case where any independent combination of insertion and rotation of the tubes as a function of time is allowed, but no groups of tubes move together, i.e. functions $\dot{\theta}_i(t)$ satisfy $\dot{\theta}_i(t) \neq \dot{\theta}_j(t)\ \forall\ i,j = 1,\ldots,n$ over an insertion, the possible solutions to equation (7) can also be divided into two cases, corresponding to the terms in equation (7) of each tube compensating individually or in conjunction.

In the case of compensating individually, equation (7) particularizes to

$$\mathbf{R}'(\theta_i)\,\mathbf{P}_i\hat{\mathbf{u}}_i^{F_i}(s-h_i)\,\dot{\theta}_i - \mathbf{R}(\theta_i)\,\frac{\partial}{\partial s}\left(\mathbf{P}_i\hat{\mathbf{u}}_i^{F_i}(s-h_i)\right)\dot{h}_i = -v\mathbf{R}(\theta_i)\,\frac{\partial}{\partial s}\left(\mathbf{P}_i\hat{\mathbf{u}}_i^{F_i}(s-h_i)\right) \qquad \forall s,t,i \quad (16)$$

Regrouping, equation (16) can be rewritten as

$$\mathbf{R}'(\theta_i)\mathbf{P}_i\hat{\mathbf{u}}_i^{F_i}(s-h_i)\dot{\theta}_i = (\dot{h}_i - v)\mathbf{R}(\theta_i)\frac{\partial}{\partial s}\left(\mathbf{P}_i\hat{\mathbf{u}}_i^{F_i}(s-h_i)\right) \quad (17)$$

which must also be satisfied for all s,t,i. Equation (17) simplifies the geometrical interpretation of the differential equation, elucidating the relation that must be satisfied between vector $\mathbf{P}_i\hat{\mathbf{u}}_i^{F_i}$ and its derivative with respect to s.

Two different design possibilities in terms of precurvatures and stiffness of the tubes comprising the robot arise from equation (17), which depend on whether the modulus of $\mathbf{P}_i\hat{\mathbf{u}}_i^{F_i} = \mathbf{q}_i$ is designed to be constant or not.

(i) If $\|\mathbf{q}_i\|$ is constant, the directions of $\mathbf{R}\partial\mathbf{q}_i/\partial s$ and $\mathbf{R}'\cdot\mathbf{q}_i$ are parallel. This implies that there can be both $\dot{h}_i(t) \neq v, 0$ and $\dot{\theta}_i(t) \neq 0$ simultaneously. In this case, the solution of equation (17) has one degree of freedom to choose from, either $\dot{h}_i(t)$ or $\dot{\theta}_i(t)$. Regardless of the choice, provided that $\dot{h}_i(t) \neq v$, equation (17) represents an ordinary differential equation analogous to that in the rotation-only case, since the difference between $\mathbf{R}_i$ and $\mathbf{R}_i'$ is again constant and equal to $\pi/2$, yielding

$$\mathbf{R}\left(\frac{\pi}{2}\right)\mathbf{P}_i\hat{\mathbf{u}}_i^{F_i}(s-h_i)\,\dot{\theta}_i = -(\dot{h}_i - v)\,\frac{\partial}{\partial s}\left(\mathbf{P}_i\hat{\mathbf{u}}_i^{F_i}(s-h_i)\right) \quad (18)$$

The solution to equation (18) is, as in the previous case, a vector $\mathbf{P}_i\hat{\mathbf{u}}_i^{F_i}$ of constant modulus, and direction rotating in the intrinsic XY plane proportionally to the arc length. In equation (18), it is patent that the choice of $\dot{h}_i(t)$ is completely equivalent to the choice of v and $\dot{\theta}_i(t)$, which determines the pace at which vector $\mathbf{q}_i$ rotates with the arc length. Hence, if $\|\mathbf{q}_i\|$ is constant, the follow-the-leader trajectories that can be obtained by combining $\dot{h}_i(t)$ and $\dot{\theta}_i(t)$ are equivalent to those achievable using $\dot{\theta}(t)$ only. Naturally, this is only valid for the segment of the robot where the tube with $\dot{h}_i(t) \neq v, 0$ is present. The combination of $\dot{\theta}_i(t)$ and $\dot{h}_i(t)$ is only advantageous in a scenario where a variation of the relative insertion of a tube is desired. Such a maneuver does not increase the variety of single trajectories that can be traced in follow-the-leader. However, it enables the linkage of some of these single trajectories, which can be useful in practical applications, as described in Section 4. The satisfaction of equation (16) for a t and any s directly implies that equation (16) is satisfied for all t, since the vector $\mathbf{P}_i\hat{\mathbf{u}}_i^{F_i}$ corresponding to each tube rotates along the arc length at a constant rate. Thus, the complete set of trajectories achievable for constant $\|\mathbf{q}_i\|$ is exactly equal as those in equation (15).

(ii) If $\|\mathbf{q}_i\|$ is not constant, then $\mathbf{R}\partial\mathbf{q}_i/\partial s$ generates a vector in a direction oblique to $\mathbf{R}'\cdot\mathbf{q}_i$. Therefore, the only solution is $\dot{h}(t) = v$, $\dot{\theta}(t) = 0$. This implies that tube i is fixed with respect to the workspace, while the rest of the robot advances. Such a configuration may seem idle in terms of follow-the-leader kinematics, as it does not contribute to the advancement of the robot. However, it shows that, once a tube has been inserted to some extent along the trajectory, it can be left fixed in that position while the rest of the robot continues forward, which is useful when linking trajectories composed of

different numbers of tubes. It should be noted that a configuration with $\dot{h}_i(t) = v$ cannot be simultaneously adopted in all tubes since there must be at least one tube that advances the robot's distal end (functions $h(t)$ are defined to be non-negative with respect to the robot's distal end). It is immediate to see that the solution identified for the design alternative (ii) holds for all times and cross-sections.

In the case of compensating in conjunction, specific control inputs $\dot{\theta}_i$ and $\dot{h}_i$ together with specific designs can also satisfy equation (7). This can be elucidated by rewriting equation (7) using the definition $\mathbf{q}_i = \mathbf{P}_i \hat{\mathbf{u}}_i^{F_i}$ as

$$\sum_{i=1}^{n} \mathbf{R}(\theta_i) \left[\mathbf{R}\left(\frac{\pi}{2}\right) \mathbf{q}_i (s - h_i) \dot{\theta}_i + (v - \dot{h}_i) \frac{\partial}{\partial s} (\mathbf{q}_i (s - h_i)) \right] = 0 \quad (19)$$

which must hold for all s, t.

Equation (19) is a sum of planar vectors with a relative orientation that varies with t owing to the different $\mathbf{R}(\theta_i(t))$ in different tubes. The magnitude of these vectors at each instant of time is determined by $\dot{\theta}_i$ for vectors $\dot{\theta}_i \mathbf{q}_i$, and by $\dot{h}_i$ for vectors $\dot{h}_i \partial \mathbf{q}_i / \partial s$. Thus, for a general design in a given cross-section, $\dot{\theta}_i$ and $\dot{h}_i$ of a set of tubes $i \in l$ can be selected at each instant of time so that the sum of the corresponding terms in equation (19) is zero, despite changes in relative orientation of the vectors.

The selection of $\dot{\theta}_i(t)$ and $\dot{h}_i(t)$ enables the satisfaction of equation (19) in a specific cross-section. However, $\dot{\theta}_i(t)$ and $\dot{h}_i(t)$ affect all cross-sections. For follow-the-leader to be satisfied in all cross-sections, the arrangement of vectors $\mathbf{q}_i$ and $\partial \mathbf{q}_i / \partial s$ corresponding to tubes $i \in l$, in terms of relative orientation and relative magnitude of the vectors, must be proportional in all cross-sections, in an equivalent manner as in the previous subsection. The corresponding design of the tubes is then equal to that in the previous subsection, with $\mathbf{P}_i \hat{\mathbf{u}}_i^W$ and $\partial \mathbf{P}_i \hat{\mathbf{u}}_i^W / \partial s$ for tubes $i \in l$ that must have a magnitude that varies exponentially along the arc length, and an absolute orientation either constant or rotating at a constant rate along the arc length. The trajectories that can be traced in a follow-the-leader configuration by compensating in conjunction using $\dot{\theta}_i$ and $\dot{h}_i$ are then equal to those in the previous subsection (equation (14)).

Compensating in conjunction involves two or more tubes. Configurations with two tubes lead to a robot with two degrees of freedom, as four inputs ($\dot{\theta}_1$, $\dot{\theta}_2$, $\dot{h}_1$, $\dot{h}_2$) are available to satisfy the two equations implied by equation (19). Any additional tubes add two degrees of freedom per tube. Thus, even though the use of both $\dot{\theta}_i$ and $\dot{h}_i$ does not increase the follow-the-leader trajectories with respect to those traceable using $\dot{\theta}_i$ only, the use of both $\dot{\theta}_i$ and $\dot{h}_i$ provides additional degrees of freedom. These degrees of freedom imply that either $\dot{\theta}_i$, $\dot{h}_i$, or a combination of them can be used to maintain follow-the-leader, as in the previous case, involving tubes compensating individually with $\dot{\theta}_i$ and $\dot{h}_i$. As before, this applies to the region of robot that contains the tubes with $\dot{\theta}_i$ and $\dot{h}_i$. The exploitation of these kinematics combining $\dot{\theta}_i$ and $\dot{h}_i$ is described in Section 4.

It should be noted that the trivial solution $\dot{h}(t) = v$, $\dot{\theta}(t) = 0$ also satisfies equation (19) for any general design $\mathbf{q}_i$. As in the previous case, this solution does not contribute to the advancement of the robot in a follow-the-leader configuration, but it can be exploited in the additional kinematics described in Section 4.

The previous discussion for both configurations compensating individually or in conjunction shows that the use of the relative tube's insertion as control input $\dot{h}_i(t)$ does not contribute to the enhancement of the set of trajectories where follow-the-leader is possible. An alternative argument for discarding relative tube insertion from contributing to follow-the-leader kinematics is that any positive $\dot{h}_i(t)$ motion prevents tube i from remaining at the robot's distal end, and any negative $\dot{h}_i(t)$ implies a certain offset until the eventual instant of time when the tube becomes part of the distal end. Thus, a tube with $\dot{h}_i(t) \neq 0$ could only contribute to the distal end's kinematics during an instant of time. Nonetheless, the strategy of using $\dot{h}_i(t) = v$ remains useful for the linkage of trajectories achieved with different numbers of tubes, as previously mentioned.

In the case of compensating individually, the control input for each tube is also restricted by equation (17). To satisfy equation (17) at a given time instant, a specific tube geometry must be selected, as previously discussed. Once the geometry is specified, equation (17) imposes a constant relation between $\dot{\theta}(t)$, $\dot{h}(t)$, and v at each section for any time. Assuming constant stiffness of the tubes for simplicity, this relation can be written as

$$\dot{\theta}_i + (\dot{h}_i - v) w_i = 0 \quad (20)$$

where w_i is the torsion of the tube expressed in m^{-1}.

Equation (20) corresponds to the control input required in each individual tube to satisfy the follow-the-leader condition (equation (17)). Equation (20) elucidates the aforementioned freedom in the follow-the-leader control of each individual tube, where different combinations of $\dot{\theta}_i(t)$ and $\dot{h}_i(t)$ satisfy equation (18) and, similarly, equation (17). However, $\dot{h}_i(t)$ must be either zero or v in the follow-the-leader configurations where the robot advances in order to satisfy the requirements on curvature discontinuities described in Subsection 3.2. Thus, the relation between $\dot{\theta}_i(t)$ and v is constant and determined by the geometry of the specific tube in the scenarios where the robot advances, with a specific rotation rate of each tube relative to the insertion rate. In particular, each advancing tube must rotate at a rate of w_i relative to the arc length. A common example of such a configuration is found in the insertion of a corkscrew, where the rotation rate relative to the insertion is determined by the helix geometry.

In the case of compensating in conjunction, the required control inputs $\dot{\theta}_i(t)$, $\dot{h}_i(t)$ to maintain follow-the-leader motion can be determined from equation (19). In some

cases, however, this can be complicated, and may lack insight into the mechanics of the robot. Alternatively, considering that the evolution of $\mathbf{u}_T^W(s_0,t)$ at any cross-section s_0 is known for each trajectory (equation (14)), equation (4) can be used to determine $\theta_i(t)$, $h_i(t)$ and thus $\dot{\theta}_i(t)$, $\dot{h}_i(t)$. $\theta_i(t)$ and $h_i(t)$ are the angles and insertions that satisfy that the sum of vectors $\mathbf{P}_i\hat{\mathbf{u}}_i^W(s)$ at a cross-section is equal to the resulting curvature for all t. The control inputs determined for a cross-section then apply to the entire robot, since the relative orientation and relative magnitude of $\mathbf{P}_i\hat{\mathbf{u}}_i^W$ and $\partial\mathbf{P}_i\hat{\mathbf{u}}_i^W/\partial s$ in each cross-section must remain proportional along the robot's arc length for each set of tubes compensating in conjunction, as previously discussed.

The degrees of freedom of the control inputs can be seen in equation (4), where both $\dot{\theta}_i(t)$ or $\dot{h}_i(t)$ can be selected to achieve the desired evolution for the resulting curvature (equation (14)). As previously mentioned, the conditions on curvature discontinuities imply that the insertion inputs must be $\dot{h}_i = 0$ or $\dot{h}_i = v$ for a concentric tube robot to maintain follow-the-leader motion over the entire robot. Then, only $\theta_i(t)$ can be used to follow the resulting curvature (equation (14)). Interestingly, in designs composed of two tubes, the $\theta_i(t)$ then involve the curvature vectors of both tubes monotonically tending toward an aligned or opposed configuration.

The condition for follow-the-leader (equation (7)) is a sum of terms corresponding to different tubes. Therefore, as in Subsection 3.3.1, combinations of configurations that involve compensating individually and compensating in conjunction also satisfy equation (7). The complete set of trajectories that can be traced in a follow-the-leader configuration under the assumptions of this second case is then equal to that in the previous subsection (equation (15)). The only extension in terms of follow-the-leader motion is the possibility of leaving tubes static relative to the workspace while the rest of the robot advances.

3.3.3. General configuration including groups of tubes. Considering now the most general case, where any control inputs are allowed, the solutions to equation (7) are generally equivalent to those in the previous case, with the exception of configurations where groups of tubes move with a common $\dot{\theta}_i(t)$. These configurations are discussed in the following, both for groups of tubes compensating individually and in conjunction with other groups.

In the case of each group compensating individually, the terms of each group must then satisfy

$$\mathbf{R}'(\theta_j)\sum_{i=1}^{m}\mathbf{q}_i(s-h_i)\dot{\theta}_j-\mathbf{R}(\theta_j)\sum_{i=1}^{m}\frac{\partial\mathbf{q}_i}{\partial s}(s-h_i)\dot{h}_i = -v\mathbf{R}(\theta_j)\sum_{i=1}^{m}\frac{\partial\mathbf{q}_i}{\partial s}(s-h_i) \qquad \forall s,t \quad (21)$$

where $\theta_j(t)$ represents the common motion of the group of tubes, and m is the number of tubes in the group. Equation (21) admits various solutions, which can be divided into different configurations.

(i) If $\dot{\theta}_j(t)=0$, two possible solutions arise. First, equation (21) can be satisfied by selecting $\dot{h}_i(t)=v$ for all tubes, which is an analogous situation to that discussed in Subsection 3.3.2 case (ii).
Alternatively, by selecting a specific $\dot{h}_i(t)$ for each tube, it is also possible to satisfy equation (21) at each instant of time in a given cross-section. This solution requires at least two tubes, since two inputs $\dot{h}_i(t)$ are necessary to satisfy equation (21) for all t. In the case of the group of tubes coinciding with the robot's distal end, $\dot{h}_i(t)$ of one tube must always be zero by definition of $h_i(t)$, and then three tubes are necessary. The condition that $\dot{h}_i \neq 0$ implies that the arguments of $\mathbf{q}_i$ vary with t. The inputs $\dot{h}_i(t)$, however, apply to all cross-sections. Thus, the configuration of vectors $\mathbf{q}_i$ and $\partial\mathbf{q}_i/\partial s$ must be proportional in all cross-sections to satisfy equation (21) for all s, t. The resulting trajectories are then equivalent to those described in Subsections 3.3.1 and 3.3.2. It should be noted that this solution enables one to maintain follow-the-leader motion in the part of the robot where the tubes with $\dot{h}_i(t)\neq 0$ are present, which cannot be all tubes of a robot for a sustained period of time.

(ii) If $\dot{h}_j(t)=0$, then it is necessary for $\dot{\theta}_j(t)\neq 0$, as well as $h_j(t)=0$, so equation (21) transforms as

$$\mathbf{R}'(\theta_j)\sum_{i=1}^{m}\mathbf{q}_i(s)\dot{\theta}_i = -v\mathbf{R}(\theta_i)\sum_{i=1}^{m}\frac{\partial\mathbf{q}_i}{\partial s}(s) \qquad \forall s,t \quad (22)$$

which is equivalent to case (ii) of Subsection 3.3.2, so no new trajectories are added.

(iii) If $\dot{h}_i(t)\neq 0$ and $\dot{\theta}_j(t)\neq 0$, two possible solutions arise. First, by selecting $h_i(t)=h_j(t)$ for all i,j, equation (21) becomes analogous to equation (16). Then a solution exists where the group of tubes becomes equivalent to a single tube with the geometry and stiffness of the group in equilibrium, and thus the trajectories that can be traced in a follow-the-leader configuration are equivalent to those in Subsection 3.3.2.
Alternatively, by selecting specific $\dot{h}_i(t)$ for each tube at each instant of time, equation (21) can be satisfied. This configuration is analogous to the previous case (case (i) of this subsection) for $\dot{h}_i(t)\neq v$, and therefore the trajectories that can be followed are equivalent to those in the previous case.

In the case of various groups of tubes compensating in conjunction, the groups must satisfy

$$\sum_{j=1}^{g'}\left(\mathbf{R}(\theta_j)\sum_{i=1}^{l_j}\left[\mathbf{R}\left(\frac{\pi}{2}\right)\mathbf{q}_i\dot{\theta}_j+\left(v-\dot{h}_i\right)\frac{\partial}{\partial s}(\mathbf{q}_i)\right]\right) = 0 \qquad \forall s,t \quad (23)$$

where g' is the number of groups compensating in conjunction, l_j denotes the number of tubes in group j, and arguments $\mathbf{q}_i(s - h_i)$ apply to $\mathbf{q}_i$, although they are omitted for brevity. Equation (23) is analogous to equation (19). The possible solutions can be divided into two further cases.

(iv) If $\dot{h}_i(t)$ are common for all tubes in each group, then the groups act as single tubes with a geometry and stiffness equivalent to the combination of tubes in the group. The various groups can then compensate in conjunction in an analogous manner as in the previous subsection for the case of single tubes compensating in conjunction. Hence, no trajectories are added.

(v) If the $\dot{h}_i(t)$ are different for the various tubes in each group, then the values of $\dot{h}_i(t)$ at each instant of time can be selected, either to achieve a desired evolution for the sum of terms in equation (23) corresponding to each tube so that the combination of tubes satisfies equation (23), or directly to satisfy equation (23) with the combination of terms from each individual tube. In either case, the arguments of vectors $\mathbf{q}_i$ and $\partial\mathbf{q}_i/\partial s$ at each cross-section vary, owing to the different $\dot{h}_i(t)$. Specific control inputs are then required at each instant of time to satisfy equation (23) in a cross-section, which represents a case analogous to that in Subsection 3.3.2 when compensating in conjunction. Thus, the configuration of vectors $\mathbf{q}_i$ and $\partial\mathbf{q}_i/\partial s$ must be proportional along the arc length, and the resulting trajectories are equivalent to those in Subsection 3.3.2.

From the discussion in this subsection, it can be concluded that the combination of a group of tubes with a common $\theta_i(t)$ does not expand the trajectories feasible in follow-the-leader configurations from those derived in the previous subsections. Nonetheless, the fact that groups of tubes moving in conjunction are equivalent to a single tube can be useful for the insertion of various tubes with singular precurvatures that cannot be inserted individually in a follow-the-leader configuration, but that in conjunction result in a geometry that can satisfy follow-the-leader. The exploitation of this configuration is considered and developed in the additional maneuvers described in Section 4. It should be noted that the control input required for the insertion of a group of tubes is that corresponding to the single tube equivalent to the group, elucidated in equation (20).

3.3.4. Curvature discontinuities. Up to this point, the study of trajectories where follow-the-leader is possible considered only continuous curves satisfying equation (6). However, trajectories with curvature discontinuities can also be traced in a follow-the-leader configuration, provided that the conditions described in Subsection 3.1 are satisfied. An example is the well-established trajectory composed of circumference arcs (Sears and Dupont, 2006).

In general, the points of curvature discontinuity must remain in a constant position in the workspace, which implies that they must translate at velocity v away from the robot's distal end as it advances. This requires the tubes causing the discontinuity to have $\dot{h}_i(t) = v$ from the point where the trajectory discontinuity is reached, onward. Considering that discontinuities appear at either the end of a tube or a discontinuous precurvature of a tube, follow-the-leader motion in trajectories with discontinuities is made possible by leaving one or more tubes fixed at each point of curvature discontinuity while the rest of the robot proceeds forward. Each segment of trajectory between curvature discontinuities must satisfy equation (7). Thus, the complete trajectory must be a combination of segments of the trajectories identified in the previous subsections. These combined trajectories are discussed in more detail in Subsection 4.1.

3.4. Set of trajectories summary

The trajectories found in Subsections 3.3.1 to 3.3.3, together with their combinations in Subsection 3.3.4, constitute the set of trajectories that can be traced in a follow-the-leader configuration, since all possible cases solving equation (7) have been considered, in addition to curvature discontinuities. The trajectories, excluding combinations of them, can be synthesized in a single expression

$$\mathbf{u}_T^W(s,t_f) = \sum_{i=1}^{n'} \begin{bmatrix} \left\|\mathbf{P}_i\hat{\mathbf{u}}_i\right\| \cos(w_i s + \phi_i) \\ \left\|\mathbf{P}_i\hat{\mathbf{u}}_i\right\| \sin(w_i s + \phi_i) \\ 0 \end{bmatrix} + \sum_{j=1}^{g} \begin{bmatrix} e^{\lambda_j s} \left\|\mathbf{u}_{R,j}\right\| \cos(\rho_j s + \nu_j) \\ e^{\lambda_j s} \left\|\mathbf{u}_{R,j}\right\| \sin(\rho_j s + \nu_j) \\ 0 \end{bmatrix} \quad (24)$$

where $\left\|\mathbf{P}_i\hat{\mathbf{u}}_i\right\|$, w_i, $\left\|\mathbf{u}_{R,j}\right\|$, λ_j, and ρ_j are selected in the robot design, and ϕ_i and ν_j are determined by the rotational orientation of the tubes at the beginning of the trajectory. The modulus $\left\|\mathbf{P}_i\hat{\mathbf{u}}_i\right\|$ must be constant according to the previous discussion, but its value can be chosen as desired by selecting an appropriate initial stiffness and curvature for each tube. Similarly, the $\left\|\mathbf{P}_i\hat{\mathbf{u}}_i\right\|$ of the tubes that compensate in conjunction to create $\left\|\mathbf{u}_{R,j}\right\|$ must vary exponentially, but the rate λ_j and the magnitude of $\left\|\mathbf{u}_{R,j}\right\|$ can be selected as desired with the design of these tubes. The values of w_i and ρ_j, which correspond to the initial torsion of either tubes i or j, can also be freely selected provided that they are constant.

The initial designs of the individual tubes or groups of tubes comprising a concentric tube robot capable of follow-the-leader motion must satisfy $\mathbf{P}_i\hat{\mathbf{u}}_i^{F_i}$ and $\partial\mathbf{P}_i\hat{\mathbf{u}}_i^{F_i}/\partial s$ to remain proportional along the arc length, as discussed in the previous subsections. In the case of compensating in conjunction, the relative orientation and proportionality of $\mathbf{P}_i\hat{\mathbf{u}}_i^{F_i}$ and $\partial\mathbf{P}_i\hat{\mathbf{u}}_i^{F_i}/\partial s$ must be equal for all tubes that compensate. Interestingly, for the common configuration of tubes with constant stiffness along the arc length, the initial geometry of the tubes that compensate individually is a helix, whereas that of tubes that compensate in conjunction is a deformed helix with continuously varying curvature magnitude. A particular case of degenerated helix is a

circumference arc. Thus, equation (24) includes the well-established robot designs consisting of constant-curvature tubes. It should be noted that the use of helical tubes has been previously introduced in Gilbert et al. (2015). In this work, the concept is extended and formalized by deriving it from a general study, as described in the previous subsections.

The robot designs corresponding to equation (24), however, are not limited to tubes with helical precurvatures. If tubes with variable stiffness are used, the precurvatures can present more general geometries that correspond to the deformation of helices, provided that the aforementioned relations on $\mathbf{P}_i\hat{\mathbf{u}}_i^{F_i}$ are satisfied. These designs are equivalent to those of constant-stiffness tubes in terms of follow-the-leader capabilities, but they can be exploited in additional maneuvers described in the next section, which combine follow-the-leader motion with other general kinematics in different parts of the robot, to increase the possibilities of motion and geometry in the parts of the robot that do not remain in a follow-the-leader configuration.

It should be noted that $\mathbf{P}_i$ is a non-dimensional stiffness determined by the stiffnesses of all tubes comprising a robot. In this regard, the design of the tubes in a robot is not decoupled, and instead a concentric tube robot must be designed, considering all the tubes that comprise it. In addition, in the case of configurations including tubes with $\lambda_j \neq 0$, which involve compensating in conjunction, two or more tubes are required for each term that involves a specific set of λ_j and ρ_j in the trajectories (equation (24)).

Equation (24), together with combinations of the trajectories linked as introduced in Subsection 3.3.4, represent the complete set of trajectories that can be traced in follow-the-leader motion under the assumption of no axial torsion of the tubes. A broad variety of trajectories can therefore be followed. However, it should be noted that a generic robot design cannot be used to follow any desired trajectory in the set (equation (24)), and instead a robot must be designed to follow a desired, small subset of the trajectories determined by variations in the ϕ_i, ν_j and the insertion lengths of the tubes. In the particular case of using a robot with the minimum number of tubes necessary to follow a desired trajectory, the desired trajectory would require a specific robot design in terms of the initial $\mathbf{P}_i\hat{\mathbf{u}}_i$ of the tubes. It should also be noted that the length of trajectories involving terms with $\lambda \neq 0$ is typically limited, as the curvature in these terms increases exponentially, rendering the trajectories prone to instability and of limited practical interest.

The control input required in each tube or group of tubes to maintain follow-the-leader motion over an entire concentric tube robot is given by equation (20) with $\dot{h}_i(t) = 0$ for all tubes that are advancing and compensating individually in a possibly combined trajectory. The inputs required in tubes or groups of tubes compensating in conjunction is also $\dot{h}_i(t) = 0$, and a value of $\theta_i(t)$ that can be determined from equation (4), so that the curvature resulting from the tubes compensating in conjunction follows the evolution of the corresponding term in equation (24). In both cases, the control input for tubes that remain stationary at the end of a segment of a combined trajectory is $\dot{h}_i(t) = v$, $\dot{\theta}_i(t) = 0$.

The set of trajectories summarized in equation (24) is broad, and torsion can be expected to occur in some of the trajectories. This can render some of the trajectories partially inaccurate or completely unfeasible, as studied in Section 5. Before the analysis of torsion, additional kinematics of interest are considered in the following section, completing the general study of motion related to follow-the-leader.

4. Additional maneuvers

The kinematic analysis presented up to this point focused on follow-the-leader motion. However, some potentially exploitable kinematic possibilities were also found in the discussion. The applicability of these kinematics, together with additional motions related to follow-the-leader motion, are described in this section. The majority of these kinematics have been previously proposed in the literature for robots comprising a set of piecewise constant-curvature tubes. This work simply extends some of these kinematic possibilities to the new trajectories found here, and integrates them into the derivation in this paper to complete the analysis.

4.1. Trajectory linking

The possibility of inserting one or more tubes that compose a robot with $\dot{h}_i = 0$, $\dot{\theta}_i \neq 0$, and, at a certain point, switching the control of some of these tubes to $\dot{h}_i = v$, $\dot{\theta}_i = 0$, was mentioned in Subsection 3.3.2. This involves inserting one or more tubes to some extent together with the rest of the robot, and leaving these specific tubes fixed at a certain point while the rest of the robot proceeds forward, maintaining follow-the-leader motion throughout the entire robot (including the segment of the robot in which some tubes are left stationary).

This concept of telescopic deployment to enable follow-the-leader motion is well established in the literature (Dupont et al., 2012; Gosline et al., 2012) and was originally introduced a decade ago by Sears and Dupont (2006) for tubes with piecewise constant curvature. In this work, the concept is extended to general trajectories composed of segments of trajectories from the equation (24). More specifically, this deployment strategy can be exploited to follow trajectories in which the geometry of the first segment is determined by equation (24) for any desired number of tubes with selected precurvatures, and the geometry of the subsequent segments corresponds to equation (24) for equal precurvatures but a reduced number of tubes. In this manner, different trajectories from the set summarized in equation (24) can be linked and followed with a single robot, expanding the follow-the-leader kinematics. The

telescopic insertion of tubes with piecewise constant curvature and no torsion is included as a particular case of linked trajectories. However, this deployment strategy is applicable to the broader set of trajectories discovered in this work (equation (24)).

The linkage of trajectories also enables the reachability of concentric tube robots to be extended. Tubes with significant precurvatures, which are generally prone to torsional instability, can be inserted a short length at the beginning of the trajectory, while tubes with shallower precurvatures can proceed forward. This is particularly relevant in keyhole surgery, where reaching a desired location can require follow-the-leader motion in regions with clearly differentiated kinematic requirements. Typical examples can be scenarios where entry into the body at a specific angle is a challenge, and the subsequent trajectory requires shallower curvatures, as can be the case of interventional magnetic resonance procedures where access to the patient within the bore of the scanner is restricted. Specific examples of this can be focal ablation, brachytherapy, tissue sampling, or drug delivery, performed under live magnetic resonance imaging.

4.2. Combined follow-the-leader and general motion

One of the results drawn from the analysis in Subsection 3.3 is that both $\dot{\theta}_i$ and $\dot{h}_i$ can be used to maintain follow-the-leader motion in the parts of the robot where the tubes with $\dot{\theta}_i$ and $\dot{h}_i$ are present. This applies both to configurations compensating individually, where it leads to one degree of freedom per tube, and configurations compensating in conjunction, where it leads to $2l - 2$ degrees of freedom. Once a robot has been inserted, it is then possible to operate individual tubes (or subsets of tubes in the case of compensating in conjunction) independently by using $\dot{h}_i \neq v, 0$ and the corresponding control input $\dot{\theta}_i$, determined from equation (20), for tubes compensating individually, or from equation (4), for tubes compensating in conjunction, as previously described. Follow-the-leader motion is then maintained throughout the part of the robot that contains the tubes controlled with $\dot{h}_i \neq v,\ 0$. Similarly, it is possible to independently operate some of the tubes composing a group that has been inserted with common $\dot{\theta}_i$ and $\dot{h}_i$, and maintain follow-the-leader motion provided that their individual design satisfies equation (17), or that the combination of designs of a subset of the tubes in the group satisfies equation (19). In the case of a tube or subset of tubes satisfying the design requirements for follow-the-leader motion in their proximal region only, their independent operation enables follow-the-leader motion in the part of the robot that contains the corresponding region of the tubes.

These kinematic equivalences enable general motion of the robot's distal part while maintaining a follow-the-leader configuration of the body of the robot once it has been inserted. In particular, there exist two main alternatives. The first involves varying the insertion of a tube or a subset of tubes using follow-the-leader control in a configuration where the tubes being actuated present some offset $h_i > 0$, i.e. the tubes are not at the robot's distal end. This leads to general, transversal motion of the robot's distal segment $s \in [0, h_i]$, while the rest of the robot, which contains the tube being actuated, remains in a follow-the-leader configuration. The second alternative involves using a group of tubes that satisfies the design requirements for follow-the-leader as a group, but is composed of tubes that, either individually or in conjunction for a subset of the tubes in the group, only satisfy the follow-the-leader requirements in the proximal part of the robot, presenting a general design in the distal part of the robot. In this configuration, the independent operation of the tubes using a follow-the-leader control corresponding to the proximal region of the tubes also enables follow-the-leader motion in the proximal part of the robot, combined with general motion of the distal region of the robot. The selection of the general curvature function in the distal part of the individual tubes determines the general motion generated at the robot.

It should be noted that the strategy of maintaining the proximal part of the robot in a steady configuration while the distal part is used as a manipulator was already proposed by Dupont et al. (2010b). In this regard, the contribution of this work is to expand the strategies to achieve this type of motion as well as the possible trajectories and kinematics under a common framework.

A relevant advantage of the kinematics proposed in this subsection, in particular, the use of groups of tubes, is that, during the insertion, the group behaves as a single tube with $\theta_i(t) = \theta_j(t)$. Thus, it can contribute to the follow-the-leader kinematics during the robot insertion, reducing the number of tubes required, and then the group can be split for general maneuvers. Furthermore, the kinematics described in this subsection enable smooth variations of the robot's distal end configuration during insertion, which do not correspond to a follow-the-leader configuration. These can be particularly useful during insertions through soft tissue where trajectory corrections are required.

4.3. Idle tubes

The quasistatic model (equation (4)) shows that the combination of two tubes with opposite precurvatures results in a tube with zero curvature since the tubes' curvatures compensate at each cross-section. Thus, a tube with a general desired curvature near the distal end and a straight geometry toward the proximal end can be integrated in a robot as a straight tube by combining it with its opposite, in an idle configuration shown in Figure 3(a). The incorporation of the resulting straight tube does not affect the possibility of follow-the-leader motion; it simply increases the robot's stiffness.

Once the robot is inserted, the idle tubes can be activated by modifying their relative rotation or insertion, as shown in

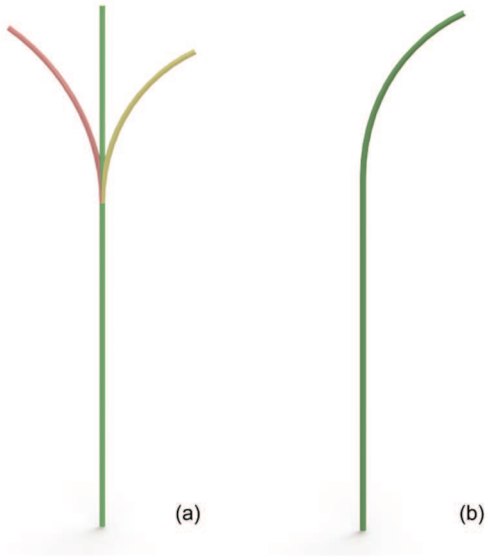

Fig. 3. Idle tubes concept corresponding to: (a) two tubes (red and yellow) with opposite curvatures, resulting in a straight geometry (green) useful for insertion; (b) the same tubes with aligned curvatures, which corresponds to an active configuration with bending in the segment near the distal end.

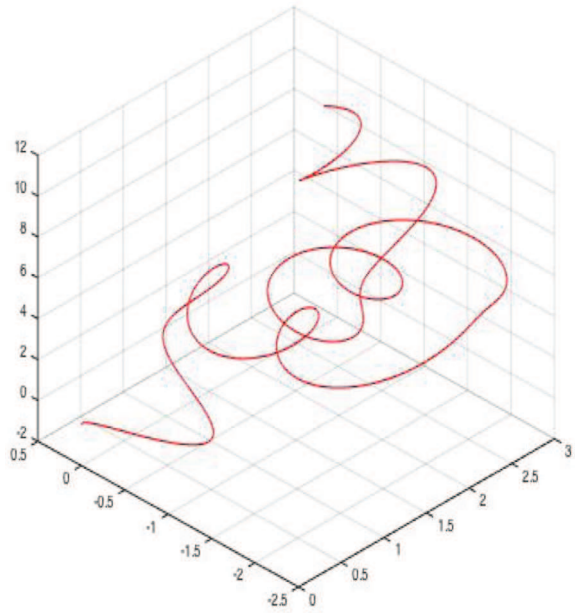

Fig. 4. Example of trajectory from the set (equation (24)), illustrating the fact that the assumption of no axial torsion can lead to intriguing predictions, but a study of torsion is required to determine feasibility.

Figure 3(b). The active tubes only present curvature in the segment near the distal end, which is determined by their design. The result is the possibility of general motion at the robot's distal end once inserted, while maintaining a follow-the-leader configuration throughout the rest of the robot. The general motion achievable at the distal end is determined by the geometry of the idle tubes, which is selected by design. As in the previous subsections, the idea of using idle tubes has been proposed previously in the literature. Here, the idea is generalized to the precurvatures and trajectories discovered in this paper, and the concept is extracted from the analysis in the previous sections, leading to a more complete study.

The advantage of using idle tubes relative to the maneuvers described in the previous subsection is that idle tubes do not impose any restrictions on their control, since their proximal part is straight. Conversely, idle tubes cannot contribute to the follow-the-leader kinematics, unlike the groups of tubes described in the previous subsection. In this regard, idle tubes lead to a noticeable increase in robot stiffness, requiring higher precurvatures in the robot design to follow a specified trajectory. This results in devices prone to torsional instability, which is discussed in Section 5. Thus, the practical applicability of the idle tubes concept is relatively limited.

5. Torsion

The analysis presented in the previous sections is predicated on the assumption of no axial torsion of the tubes composing the robot. Such an assumption can be used in the kinematic study of concentric tube robots, and it leads to the solutions described in previous sections. However, a certain degree of torsion is generally present in concentric tube robots, and therefore a certain deviation from follow-the-leader can occur in the trajectories previously identified. When torsion is significant, concentric tube robots can even become unstable in some of the previously identified trajectories, owing to the so-called snap-through instability described in Dupont et al. (2010b). Thus, even though some of the trajectories found under the assumption of no torsion can be tempting, as that shown in Figure 4, they may not be viable.

The torsion of concentric tube robots is studied in this section to determine the validity of the assumption of no axial torsion, and therefore allow for the selection of robot configurations where such an assumption is an acceptable approximation. The study of torsion requires a general equilibrium analysis, which is derived in this section using special Cosserat rod equilibrium theory, following the approach in Dupont et al. (2010b). The study is then made specific to trajectories of interest in Subsection 5.2, and a closed-form solution for a two-tube robot is presented. The implications of such a solution are subsequently discussed in Subsection 5.3, and criteria to ensure that the torsion of the tubes is less than a specified value are extracted. The relation between torsional deformation and deviation in task space is illustrated with some cases of interest in Subsection 5.4, serving for the selection of a robot design for the case study described in Section 6.

5.1. General formulation of torsional study

The derivation of the general differential equation governing torsion presented in this subsection is analogous to that in Dupont et al. (2010b). However, the main steps of the derivation are included for completeness, serving as a foundation for the subsequent analysis in this paper. To facilitate the integration of this work with existing literature, a new variable is defined, $\zeta = L - s$, which corresponds to the arc length relative to the robot's proximal end. The study of torsion in the following is derived using ζ as the independent variable.

The equilibrium of a tube i subjected to distributed external forces $\mathbf{f}$ and moments τ can be imposed as

$$\begin{bmatrix} \dot{\mathbf{m}}_i \\ \dot{\mathbf{n}}_i \end{bmatrix} = \begin{bmatrix} \tau \\ \mathbf{f} \end{bmatrix} - \begin{bmatrix} [\mathbf{u}_i] & [\mathbf{v}_i] \\ 0 & [\mathbf{u}_i] \end{bmatrix} \begin{bmatrix} \mathbf{m}_i \\ \mathbf{n}_i \end{bmatrix} \tag{25}$$

where $\mathbf{u}_i$ and $\mathbf{v}_i$ represent the angular and linear deformations, respectively, $\mathbf{m}_i$ and $\mathbf{n}_i$ denote the internal moments and forces associated with the stress in the tube cross-section, and the square brackets denote a skew-symmetric matrix. The derivatives, indicated by a dot, are relative to the arc length of the curve describing the tube centerline, ζ; all the variables are a function of ζ. The variables corresponding to a tube are expressed in the tube's reference frame, although the superscript indicating the frame is omitted for simplicity in the notation.

In this work, the focus is on the robot equilibrium resulting from the interaction between tubes. Thus, $\mathbf{f}$ and τ correspond to the forces and moments exerted on a tube by the adjacent tubes. Assuming the friction between the tubes comprising the robot to be negligible, $\tau = 0$, the equilibrium equation corresponding to the torques in equation (25) is

$$\dot{\mathbf{m}}_i = -[\mathbf{u}_i]\mathbf{m}_i - [\mathbf{v}_i]\mathbf{n}_i \tag{26}$$

Considering the derivative of the constitutive relation (equation (1)) with respect to arc length

$$\dot{\mathbf{m}}_i = \mathbf{k}_i \frac{\mathrm{d}\mathbf{u}_i}{\mathrm{d}\zeta} + \frac{\mathrm{d}\mathbf{k}_i}{\mathrm{d}\zeta}\mathbf{u}_i - \frac{\mathrm{d}(\mathbf{k}_i\hat{\mathbf{u}}_i)}{\mathrm{d}\zeta} \tag{27}$$

and combining equations (26) and (27) yields

$$\mathbf{k}_i \frac{\mathrm{d}\mathbf{u}_i}{\mathrm{d}\zeta} = -[u_i]\mathbf{m}_i - [v_i]\mathbf{n}_i - \frac{\mathrm{d}\mathbf{k}_i}{\mathrm{d}\zeta}\mathbf{u}_i + \frac{\mathrm{d}(\mathbf{k}_i\hat{\mathbf{u}}_i)}{\mathrm{d}\zeta} \tag{28}$$

The angular strains can be assumed to be the prevailing deformation modes over linear strains, following Dupont et al. (2010b), leading to

$$[\mathbf{v}_i] = \begin{bmatrix} 0 & -1 & 0 \\ 1 & 0 & 0 \\ 0 & 0 & 0 \end{bmatrix} \tag{29}$$

Recalling that the initial curvature of a tube is defined in Section 2 as the curvature of the curve corresponding to its centerline, the z component of $\hat{\mathbf{u}}_i$ is zero, and therefore the z component of $\mathrm{d}(\mathbf{k}_i\hat{\mathbf{u}}_i)/\mathrm{d}\zeta$ is null. The tubes comprising the robot can be assumed to have an annular cross-section with constant stiffness for convenience, which implies $\mathrm{d}\mathbf{k}_i/\mathrm{d}\zeta = 0$ and $k_x = k_y$. Using the constitutive relation (equation (1)), after some manipulation, the z component of equation (28) can be written as

$$\dot{u}_{iz} = \frac{k_x}{k_z}(u_{ix}\hat{u}_{iy} - u_{iy}\hat{u}_{ix}) \tag{30}$$

which describes the torsional derivative of a tube with respect to ζ as a function of its initial and deformed bending curvatures. It should be noted that this expression is equivalent to that presented in Dupont et al. (2010b), as it is applicable to any concentric tube robot design under the aforementioned assumptions.

Considering a robot composed of two tubes, the relative twist angle can be defined as

$$\alpha(\zeta) = \theta_2(\zeta) - \theta_1(\zeta) \tag{31}$$

where θ_i represents the torsional displacement of tube i. Combining the derivatives of equation (31) with equilibrium of moments (equation (2)), the constitutive law (equation (1)), and equation (30), the second derivative of the twist can be related to the initial and final curvatures of tube 2. The reader is referred to Appendix A for details. The resulting expression is

$$\ddot{\alpha} = \left(\frac{k_{2x}}{k_{2z}} + \frac{k_{2x}}{k_{1z}}\right)(u_{2x}\hat{u}_{2y} - u_{2y}\hat{u}_{2x}) \tag{32}$$

The variables u_{2x} and u_{2y} can be expressed as functions of the initial curvatures of the tubes and the relative twist using the governing equations in Section 2. Taking equation (4) in combination with equation (3), and expressing the relations in the Bishop frame associated with tube 2, F_2, considering that in such a case $\mathbf{R}(\theta_1) = \mathbf{R}(-\alpha)$ and $\mathbf{R}(\theta_2) = \mathbf{I}$, the following relations are obtained

$$\begin{aligned} u_{2x} &= \frac{1}{k_{1x} + k_{2x}}(k_{1x}\hat{u}_{1x}\cos\alpha + k_{1y}\hat{u}_{1y}\sin\alpha) \\ u_{2y} &= \frac{1}{k_{1y} + k_{2y}}(-k_{1x}\hat{u}_{1x}\sin\alpha + k_{1y}\hat{u}_{1y}\cos\alpha) \end{aligned} \tag{33}$$

Substituting equation (33) into equation (32), and after some manipulation, including the aforementioned assumption that $k_x = k_y$, the expression governing the relative twist of the tubes as a function of their initial curvatures is obtained

$$\begin{aligned} \ddot{\alpha} = &\left(\frac{k_{2x}}{k_{1z}} + \frac{k_{2x}}{k_{2z}}\right)\left(\frac{k_{1x}}{k_{1x} + k_{2x}}\right) \\ &\left((\hat{u}_{1x}\hat{u}_{2y} - \hat{u}_{2x}\hat{u}_{1y})\cos\alpha + (\hat{u}_{1x}\hat{u}_{2x} + \hat{u}_{1y}\hat{u}_{2y})\sin\alpha\right) \end{aligned} \tag{34}$$

A first boundary condition can correspond to the twist at the proximal end of the robot, i.e. at $\zeta = 0$, which can generally be used as a control input

$$\alpha(0) = \theta_2(0) - \theta_1(0) \tag{35}$$

The second boundary condition can be obtained by considering that the torsional moment at the distal end of each tube must be zero, which implies no torsion of the tubes at $\zeta = L$ and therefore

$$\dot{\alpha}(L) = 0 \tag{36}$$

It should be noted that equation (34), together with the boundary conditions (equations (35) and (36)), is general, and therefore valid for any two-tube robot design satisfying the assumptions used in the derivation.

5.2. Torsion in particular configurations

Equation (34) can be made specific to trajectories in the set (equation (24)) in order to determine the validity of the assumption of no axial torsion in practice. The most relevant trajectories in practice are those corresponding to tubes compensating individually since they only require one tube per component in equation (24), which enables a wide variety of non-trivial trajectories to be followed with a small number of tubes, and they offer lengths and curvature values of typical practical interest. The following derivation is thus focused on robots composed of tubes with helical precurvatures. Substituting these helical precurvatures from equation (24) into equation (34), and after some manipulation

$$\ddot{\alpha} = c\sin((w_2 - w_1)\zeta + \alpha(\zeta) + \phi_d) \tag{37}$$

where

$$c = \left\|\hat{\mathbf{u}}_1\right\| \left\|\hat{\mathbf{u}}_2\right\| \left(\frac{k_{2x}}{k_{1z}} + \frac{k_{2x}}{k_{2z}}\right)\left(\frac{k_{1x}}{k_{1x} + k_{2x}}\right)$$

in which $\left\|\hat{\mathbf{u}}_i\right\|$ is constant considering tubes with constant stiffness, $\phi_d = \phi_2 - \phi_1$, and the boundary conditions remain equal to those in equations (35) and (36). Defining a change of variable

$$f(\zeta) = (w_2 - w_1)\zeta + \alpha(\zeta) + \phi_d \tag{38}$$

equation (37) transforms into

$$\frac{\mathrm{d}^2 f(\zeta)}{\mathrm{d}\zeta^2} = c\sin(f(\zeta)) \tag{39}$$

with boundary conditions

$$\begin{aligned} f(0) &= \alpha(0) + \phi_d \\ \dot{f}(L) &= w_2 - w_1 \end{aligned} \tag{40}$$

Equation (39), with boundary conditions (40), is similar to that obtained in Dupont et al. (2010b), but differs in one of the boundary conditions, requiring a different solution. The solution to equation (39), and its application to solve equation (37) by reversing the change of variable in equation (38), are derived in Appendix B.

Thus, defining

$$b = \frac{(w_2 - w_1)^2}{2c} + \cos(f(L)) + 1$$

and $K_e = \sqrt{(2/b)}$, the closed-form solution to the relative twist $\alpha(\zeta)$ of two tubes in the trajectories where follow-the-leader motion is possible for given design parameters can be obtained in two intervals of K_e. For $0 \le K_e \le 1$

$$\alpha(\zeta) = (w_1 - w_2)\zeta - \pi - \phi_d + 2\tan^{-1}\left[\frac{sn\left((\zeta - L)\sqrt{\frac{cb}{2}} + F\left(\frac{\alpha(L) + (w_2 - w_1)L + \phi_d + \pi}{2}, K_e\right), K_e\right)}{cn\left((\zeta - L)\sqrt{\frac{cb}{2}} + F\left(\frac{\alpha(L) + (w_2 - w_1)L + \phi_d + \pi}{2}, K_e\right), K_e\right)}\right] \tag{41}$$

where $F(x, K)$ denotes the incomplete elliptic integral of the first kind, and *sn* and *cn* correspond to the Jacobi elliptic functions. And for $K_e > 1$

$$\alpha(\zeta) = (w_1 - w_2)\zeta - \pi - \phi_d + 2\sin^{-1}\left\{\frac{1}{K_e} sn\left[(\zeta - L)\sqrt{c} + F\left(\sin^{-1}\left[K_e \sin\left(\frac{\alpha(L) + (w_2 - w_1)L + \phi_d + \pi}{2}\right)\right], \frac{1}{K_e}\right), \frac{1}{K_e}\right]\right\} \tag{42}$$

where the transition at $K_e = 1$ is smooth.

It should be noted that the solution is expressed as a function of the relative twist at the distal end of the robot, instead of the proximal end as in the boundary condition (equation (35)). An equivalent result can be obtained using $\alpha(0)$ as the independent variable instead of $\alpha(L)$ following an analogous derivation. However, $\alpha(L)$ is selected as the independent variable in this case since it facilitates the discussion on torsional stability, which is the final aim of this torsional study.

5.3. Torsion discussion

The implications of equations (41) and (42) are analyzed in this subsection. The focus is on the torsional magnitude in order to determine the validity of the assumption of no axial torsion employed in the previous sections of this paper, and thus identify stable trajectories.

Equations (41) and (42) allow the determination of the relative twist at any cross-section of a two-tube robot composed of helical tubes as a function of $\alpha(L)$ as well as the robot design parameters and ϕ_d. The evaluation of equations (41) and (42) at $s = 0$ provides the relation between $\alpha(0)$ and $\alpha(L)$ for a given robot design and ϕ_d. The effect of ϕ_d on the relation between $\alpha(0)$ and $\alpha(L)$ is simply a translation of the origin about $\alpha(0) = \alpha(L)$, which is a consequence of the fact that ϕ_d corresponds to the relative rotation of the tubes at the proximal end. Since the torsional behavior of the tubes is cyclic with period 2π, the

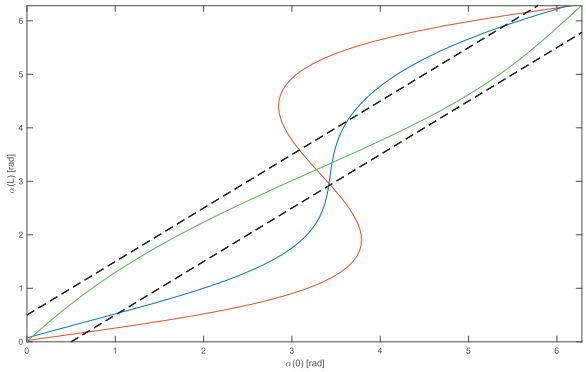

Fig. 5. Evolution of the relative twist between the distal and proximal ends of robots composed of two tubes with three different designs, which present a stable and approximately linear relation (green), a stable but non-linear evolution (blue), and an unstable behavior in the interval $\alpha(0) \in [2.8, 3.8]$.

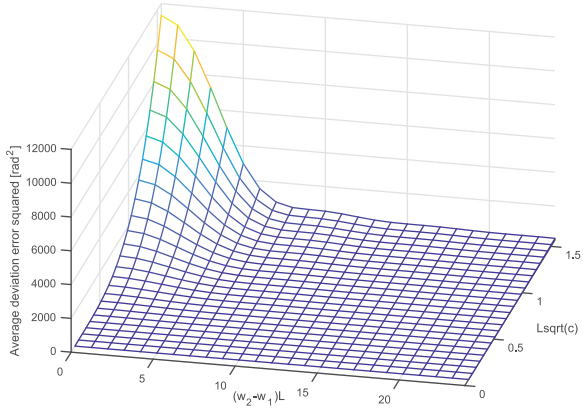

Fig. 6. Average squared deviation from $\alpha(L) = \alpha(0)$ as a function of $L\sqrt{c}$, $(w_2 - w_1)L$ in the domain of interest. The plot elucidates the trends identified, and confirms that they are monotonic in the domain of interest.

effect of ϕ_d is not relevant and is not considered further. Conversely, the influence of the design parameters on the torsional behavior is through two non-dimensional groups: $L\sqrt{c}$ and $(w_2 - w_1)L$. The relation between $\alpha(0)$ and $\alpha(L)$ can therefore be plotted for different values of the non-dimensional groups in order to study the tubes' torsional behavior.

Three illustrative examples of different relations between $\alpha(0)$ and $\alpha(L)$ are shown in Figure 5, which correspond to three different cases in terms of values of the non-dimensional groups. As can be seen, for two of the cases, the evolution of $\alpha(L)$ as a function of $\alpha(0)$ is stable, whereas in the third case the robot presents a torsional instability corresponding to a snap-through instability. The two stable examples, however, present markedly different evolutions of relative twist. The relation shown in blue is strongly non-linear, which implies that the assumption of no axial torsion is not an accurate representation of the torsional behavior. Instead, the relation shown in green is closer to linear, and therefore can be approximated well by the assumption of no axial torsion of the robot.

Studying the evolution of $\alpha(L)$ as a function of $\alpha(0)$ for a range of values of the non-dimensional groups in combination with equations (41) and (42), criteria to attain a desired torsional behavior can be extracted. The domain considered here is selected to include the configurations of practical interest, with $L\sqrt{c} \in [0, 3\pi/4]$ and $(w_2 - w_1)L \in [0, 24]$. In general, the robot is stable if $L\sqrt{c} \leq \pi/2$, although greater values can be reached in a stable manner by increasing $(w_2 - w_1)L$. Similarly, it can be seen that greater values of $(w_2 - w_1)L$ lead to a relation between $\alpha(L)$ and $\alpha(0)$ that is closer to $\alpha(L) = \alpha(0)$. The deviation from $\alpha(L) = \alpha(0)$, quantified as the average deviation error squared, is plotted in Figure 6 as a function of the non-dimensional groups in the region of stable configurations of interest $L\sqrt{c} \in [0, \pi/2]$ and $(w_2 - w_1)L \in [0, 24]$. The plot confirms the trends identified for $(w_2 - w_1)L$ and shows that they are monotonic over the region considered. Interestingly, for the case of $w_2 = w_1 = 0$, the results from equations (41) and (42) converge with the results reported by Dupont et al. (2010b). In this regard, equations (41) and (42) represent a generalization of the work in Dupont et al. (2010b) for two-tube robot designs with helical tubes, which correspond to equation (24).

A torsional deviation in the relation between $\alpha(0)$ and $\alpha(L)$ can therefore be selected to be less than a specified value in order to ensure that the assumption of no axial torsion is an acceptable approximation. It should be noted, however, that a boundary on torsional deformation does not directly imply a specific boundary on the deviation with respect to follow-the-leader motion in the resulting trajectory. The torsional deformation affects the local curvature values, whereas the deviation in the resulting trajectory is determined by the integration of the local curvature along the robot length. Thus, torsional deformation and resulting deviation in task space are related, but the relation depends on an integral.

Equations (49) and (50) can be substituted into the well-known robot model including torsion, e.g. that described in Dupont et al. (2010b), to determine the deviation in local curvature due to torsion in a two-tube robot. This can then be particularized to the robot designs and configurations found in this work to determine the local curvature deviation in the trajectories of interest (equation (24)). However, to determine the resulting position deviation due to torsion in task space, the local curvature needs to be integrated. A closed-form solution to such an integral is not available. Thus, the specific deviation in task space due to torsion cannot be directly determined from the current analysis. The possibility of approximating this integral or finding boundaries on the deviations in task space from boundaries on local curvature deviations will be addressed in future work.

Nonetheless, in some practical cases, the typical deviation in task space due to torsional deformation can be considered to follow certain trends that can be approximated for a specific family of designs based on experience. In such cases, boundaries on torsional deformation can be used to identify the trajectories where follow-the-leader is possible within an admissible deviation. To exploit any trajectories of interest, however, these must be subsequently verified to ensure that the deviation in task space is within the expected values. In more general cases, a hypothesis on the admissible torsional deformation in the specific scenario of interest can be formulated by exploring the effect of torsion on the resulting trajectory in some relevant configurations. The corresponding trajectories where approximate follow-the-leader is possible can then be identified, and trajectories of interest can be selected. However, any selected trajectory must be subsequently verified. This procedure can, therefore, require some iteration. In all cases, it should be noted that boundaries on torsional deformation typically involve using tubes with lower curvatures. In particular, in designs composed of tubes with planar precurvatures, this always applies, as torsional deformation is determined by a single parameter, $L\sqrt{c}$.

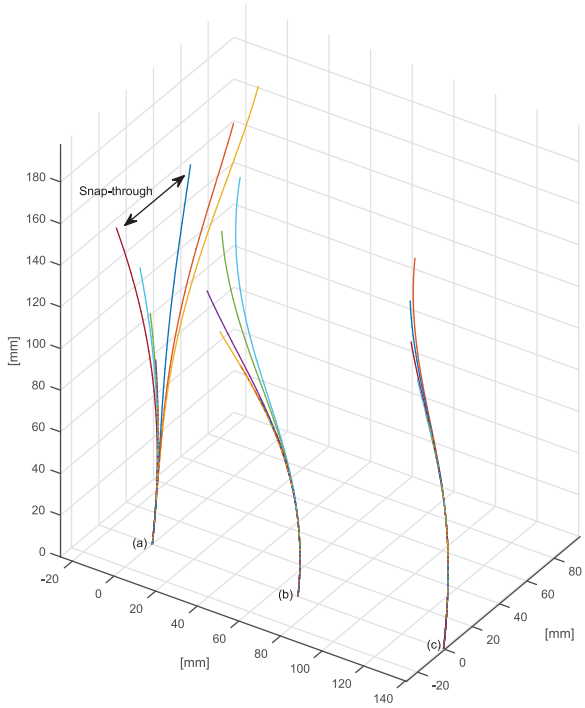

Fig. 7. Simulated insertions corresponding to three different designs: (a) significant deviation from follow-the-leader, including a snap-through instability; (b) noticeable deviation due to torsional deformation of the tubes; (c) low deviation.

5.4. Illustration of torsion effects

A set of examples of torsional deformation and the corresponding deviations in task space are presented in this subsection. These are aimed at illustrating the relation between torsion and the resulting deviation for some designs of interest.

Three simulated insertions are first used to show the behavior of three exemplary robot designs corresponding to the torsional relations shown in Figure 5, and then to quantify the follow-the-leader deviation in task space due to torsion. The simulations are implemented using the robot quasistatic model considering torsion (equation (4)) together with the solutions of torsion along the arc length (equations (41) and (42)). The robot configuration is evaluated at 10 regular intervals during an insertion. The three designs are all composed of two helical tubes with equal stiffness, a length of 20 cm, and $\|\hat{\mathbf{u}}_1\| = 11\,\mathrm{m}^{-1}$, $\|\hat{\mathbf{u}}_2\| = 8\,\mathrm{m}^{-1}$, $w_1 = 8\,\mathrm{m}^{-1}$, $w_2 = 12\,\mathrm{m}^{-1}$ for the first design, $\|\hat{\mathbf{u}}_1\| = 9\,\mathrm{m}^{-1}$, $\|\hat{\mathbf{u}}_2\| = 7\,\mathrm{m}^{-1}$, $w_1 = -12\,\mathrm{m}^{-1}$, $w_2 = 9\,\mathrm{m}^{-1}$ for the second design, and $\|\hat{\mathbf{u}}_1\| = 6\,\mathrm{m}^{-1}$, $\|\hat{\mathbf{u}}_2\| = 5\,\mathrm{m}^{-1}$, $w_1 = -18\,\mathrm{m}^{-1}$, $w_2 = 9\,\mathrm{m}^{-1}$ for the third design.

The resulting simulated insertions are shown in Figure 7. As can be seen, follow-the-leader is maintained in some parts of the trajectories, but significant deviations are present in both the first and second designs. In this work, the deviation, defined ϵ, is quantified as the maximum of the minimum distances between any point on the robot centerline at any of the configurations during an insertion and the centerline at any other configuration. The maximum deviations for the insertions shown in Figure 7 are then $\epsilon_1 = 40.7\,\mathrm{mm}$, $\epsilon_2 = 16.0\,\mathrm{mm}$, and $\epsilon_3 = 2.8\,\mathrm{mm}$, respectively. The error in these three cases thus increases with the magnitude of torsion, as can also be observed in the plots. Interestingly, the snap-through instability appears in the first design at approximately 75% of the insertion, as can be seen in Figure 7(a), where the geometry of the robot in the last three configurations is markedly different from that in the previous configurations.

Equivalent simulations can be conducted to explore the relation between torsion boundaries and deviation in task space in any set of designs. This is presented here for a relevant subset of designs corresponding to two-tube robots with helical tubes of equal stiffness, a length of 20 cm, curvatures of each tube varied within $\|\hat{\mathbf{u}}_i\| \in [3, 7]$, and torsion varied within $w_i \in [-30, 15]$, with $w_1 \neq w_2$ for each design. This subset of designs is selected as it results in trajectories of potential practical interest, which present complex geometries with variations of curvature along the arc length, in both magnitude and direction. The maximum deviation from follow-the-leader is measured in each insertion as in the previous three cases.

The maximum deviation in task space is plotted in Figure 8 as a function of the maximum torsional deviation, defined as $\Delta\alpha_M = \max \|\alpha(L) - \alpha(0)\|$ over $\alpha(0) \in [0, 2\pi]$, for all designs in the subset. As can be seen in Figure 8, the maximum deviation in task space tends to increase with the maximum torsional deformation. Interestingly, the torsional deviation of some of the designs coincides, which

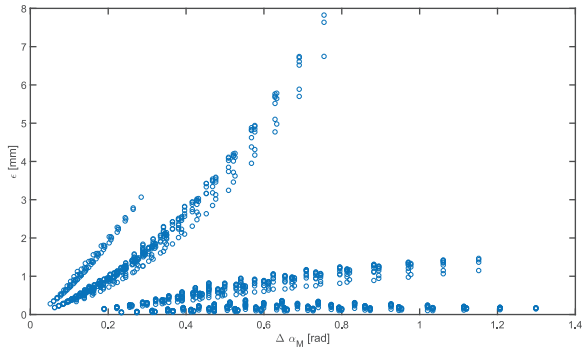

Fig. 8. Maximum deviation from follow-the-leader in task space as a function of maximum torsional deviation for a wide variety of designs.

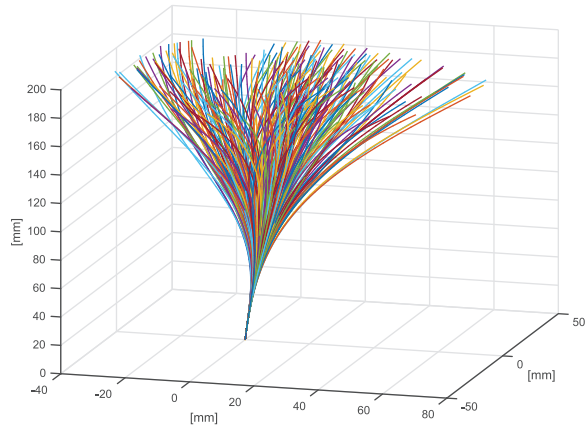

Fig. 9. Set of stable trajectories where follow-the-leader is possible using a robot composed of two tubes, with a common base pose.

is because the non-dimensional groups coincide. In some specific cases, the deviation is small despite significant torsional deviation. These are designs where w_1 and w_2 are close, and therefore the robot behaves practically as a single helix with limited relative tube rotation. Still, in the cases explored, torsion boundaries translate as bounded deviation in task space.

Torsion boundaries can then be defined in the subset of designs explored so that the assumption of no torsion is an admissible approximation, and thus the corresponding follow-the-leader trajectories can be followed within an acceptable deviation. This can be exemplified by considering admissible the relations between $\alpha(0)$ and $\alpha(L)$ that lie within two boundaries depicted as dashed lines in Figure 5, and without snap-through. These boundaries are arbitrarily set to be parallel to $\alpha(0) = \alpha(L)$ with an offset of $\pm 1/2\,\mathrm{m}^{-1}$, and correspond to maximum deviations in the task space of close to 4 mm. It should be noted, however, that these bounded deviations are only guaranteed in the specific configurations explored. Deviations on any other configuration, even if similar, must be verified.

The trajectories corresponding to the configurations explored within these bounds are plotted in Figure 9 for a common initial pose at the base. It should be noted that the trajectories shown in Figure 9 can also be rotated around the base z axis while maintaining the base pose, increasing the follow-the-leader possibilities for that pose, although they are not plotted, for clarity of illustration. It should also be noted that equations (41) and (42) do not depend on the length units in the robot design variables; therefore, any isotropic scaling of the trajectories shown in Figure 9 results in a trajectory that can also be traced in an approximate follow-the-leader manner with a deviation that scales with L. Figure 9 illustrates the potential of the trajectories discovered in this work for surgical applications, showcasing the capability of following trajectories with a continuous variation of curvature, in both magnitude and direction, in an approximate follow-the-leader configuration to reach targets in different locations from a specified initial pose.

6. Case study: simulation and experiment

The results on torsional stability presented in the previous section allow for the selection of a robot design together with a trajectory to showcase the research reported in this paper. The performance of the selected robot is presented in this section in the form of a case study involving simulation and experiment. This serves to illustrate both the capability of follow-the-leader motion in a trajectory that is unique and representative of the research on follow-the-leader control, as well as the validity of the assumption of no axial torsion in such a trajectory.

6.1. Robot design and trajectory

The case study involves a two-tube robot advancing in follow-the-leader motion along a trajectory with continuous variation of curvature, in both direction and magnitude, in the proximal part of the trajectory, and a helical geometry in the distal part. The trajectory selected is a combination of two trajectories in the set (equation (24)) linked as described in Subsection 4.1, whereby one of the tubes remains static at the linkage between trajectories while the other proceeds forward. The case study therefore serves to demonstrate the research reported in Section 3, as well as some of the work on additional exploitable kinematics described in Section 4. The behavior of the robot in the first, proximal, part of the trajectory is studied with simulations, whereas that in the second, distal, part of the trajectory is shown with an experiment.

The geometry of the complete selected trajectory can be described by the curvature κ_i, torsion w_i, and stiffness of the two tubes comprising the robot, together with their respective insertion lengths. The tube's characteristics are summarized in Table 1. The total insertion of the outer tube, tube 2, is 19 cm, whereas that of the inner tube is 26 cm. The complete trajectory is shown in Figure 10. As can be seen, it is a trajectory that cannot be followed using conventional

Table 1. Characteristics of tubes corresponding to the case study.

	κ (m^{-1})	w (m^{-1})	Outer diameter (mm)	Inner diameter (mm)
Tube 1	6.79	−26	0.9652	0.8128
Tube 2	6.22	4	1.1938	1.1176

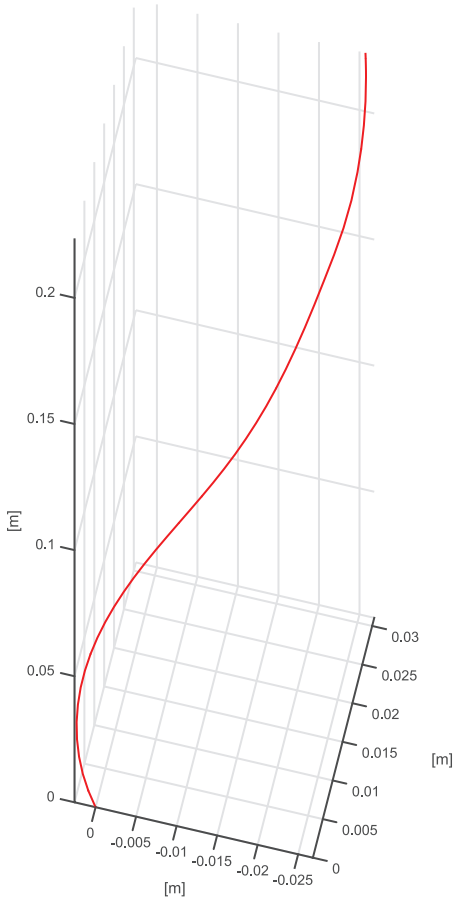

Fig. 10. Complete trajectory selected for the case study. The first, proximal, part of the trajectory presents continuous variation of curvature in both direction and magnitude; the second, distal, part of the trajectory presents a helical geometry.

constant-curvature tubes, as it presents continuous variation of curvature in the part corresponding to two tubes, and helical geometry in the part corresponding to a single tube.

The tube's characteristics are selected to minimize torsion. The evolution of $\alpha(L)$ as a function of $\alpha(0)$ can be predicted using equations (41) and (42), as shown in Figure 11. In this case, the design parameters summarized in Table 1 result in the approximately linear relation between $\alpha(L)$ and $\alpha(0)$ shown in Figure 11. Thus, torsion is expected to be low in the entire trajectory.

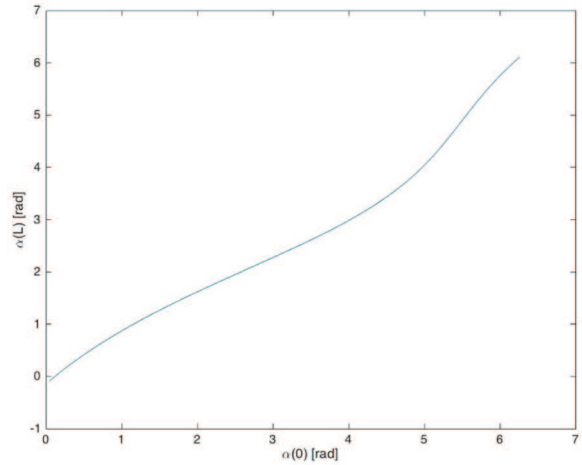

Fig. 11. Predicted evolution of the relative twist at the distal end as a function of the proximal end of the robot design selected for the experiment.

6.2. Simulation

The first part of the trajectory corresponds to both tubes advancing with $\dot{h}_1 = \dot{h}_2 = 0$ from the insertion point until full insertion of tube 2. The behavior of the robot in this part of the trajectory is studied by simulating it at a set of 20 configurations corresponding to insertion lengths between $L = 9.5$ mm and $L = 19$ cm at regular intervals. This enables evaluation of the deviation from follow-the-leader and the magnitude of torsional deformation as the robot advances.

The geometry of the robot in each of these 20 configurations is simulated as in Subsection 5.4, by combining equations (4), (41), and (42). The effects of friction between tubes and gravity are neglected, and the tubes are assumed to be made of nitinol with a Poisson ratio of $\nu = 0.33$.

The desired control inputs at the insertion point for this part of the trajectory are determined from equation (20) with $\dot{h}_i = 0$. Thus, the rotation of each tube at the insertion point should be constant and at a rate corresponding to its torsion. In practice, the tubes must be controlled by an actuation system; therefore, part of the tube will be inside this actuation system. The part of the tubes inside the actuation system may then undergo torsion as well, leading to a rotation at the insertion point different from that at the proximal ends where the tubes actuated. Considering an actuation box that constrains the tubes to remain straight inside it, the torsion in the part of the tubes inside the box is constant, according to the generalization of equation (30) for any number of tubes described in Dupont et al. (2010b). The specific torsion is then determined by the torsion at the cross-section immediately after the insertion point, $u_{iz}(\zeta = 0, t)$, which can be determined from equations (45) and (49). The desired constant rotation of θ_i at the insertion point can then be achieved with a rotation of $\gamma_i = \theta_i(\zeta = 0) - u_{iz}(\zeta = 0, t)\, d_i$ at the point where tube i is actuated, where d_i is the tube length between the point

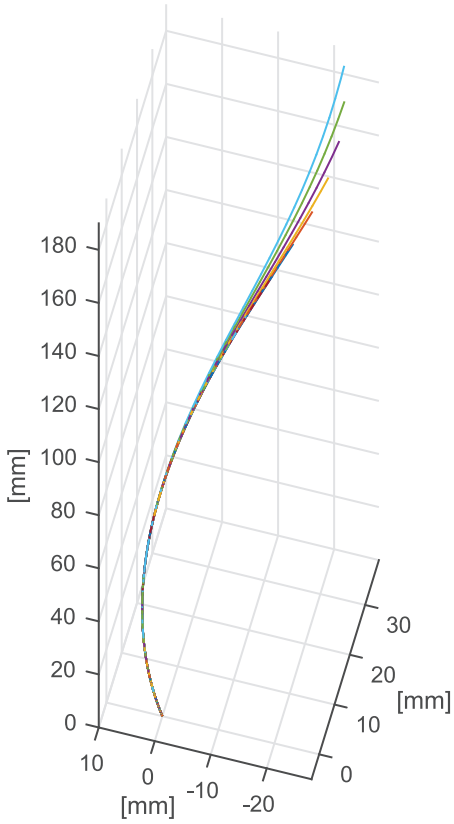

Fig. 12. Simulated insertion of robot in the first part of the trajectory.

of actuation and the insertion point. The simulations then assume ideal actuation inputs, and thus a constant rotation at the insertion point at a rate corresponding to the torsion of each tube.

The resulting simulated robot configurations are shown in Figure 12. As can be seen, an approximate follow-the-leader motion is maintained over this entire first part of the trajectory, although a certain degree of deviation is present. The deviation from follow-the-leader is relatively low near the insertion point and increases toward the distal parts of the trajectory. The maximum deviation in task space, quantified as in the previous section, is 3.5 mm, and occurs between the configurations at 85% and 100% of the insertion, at an arc length of 163.9 mm of the final configuration.

The deviations shown in Figure 12 are due to torsion. The simulated torsional deviation along the arc length $\Delta\alpha(\zeta) = \alpha(\zeta) - \alpha(0)$ is shown in Figure 13 for the robot configurations corresponding to the 20 insertion lengths. As can be seen, the torsional behavior varies as the insertion of the robot increases, which results in changes in the local curvature along the arc length, and ultimately leads to deviations from follow-the-leader in task space. The relation between deviations in local curvature and follow-the-leader error in task space is determined by the integration of curvature along the arc length, and therefore the effect of local curvature deviations is amplified with the arc length, which

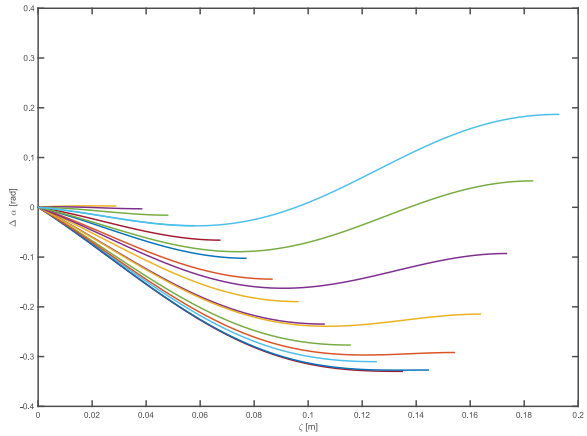

Fig. 13. Simulated torsional deviation as a function of arc length for 20 robot configurations during an insertion.

results in the larger errors in the distal parts of the trajectory shown in Figure 12.

6.3. Experiment

The second part of the trajectory is a continuation of the first one. It begins with both tubes inserted as described in the previous subsection. One of the tubes is then advanced to trace this second part of the trajectory while the other tube remains stationary relative to the task space. The robot behavior in this second part of the trajectory is demonstrated experimentally to illustrate follow-the-leader motion in practice.

The experiment starts with the distal end of both tubes coinciding, which corresponds to the end of the first part of the trajectory. Tube 1 is subsequently advanced, which involves a combination of insertion and rotation of the tube at a rate of $w_1\,\mathrm{m}^{-1}$, while tube 2 remains stationary. The geometry of the complete device is measured as tube 1 advances in order to evaluate the satisfaction of follow-the-leader motion over the entire device. The experiment proceeds until full insertion of tube 1, which corresponds to the end of the complete trajectory shown in Figure 10.

The design of the tubes used in the experiment matches the description in Subsection 6.1, summarized in Table 1. Both tubes are made of nitinol, supplied by Nitinol Devices and Components Inc., with part numbers TSE0380X0320GS and TSE0470X0440GS, respectively. It should be noted that the stiffness of both tubes is practically equal, which requires the result in equation (24) to be correct for follow-the-leader motion to occur throughout the entire robot.

Starting the experiment from the point of linkage between the two parts of the complete trajectory enables follow-the-leader motion to be achieved without the need for an actuation system. Tube 1 can be simply advanced with free rotation, relying on the elastic equilibrium of the system to rotate it naturally at the required rate w_1.

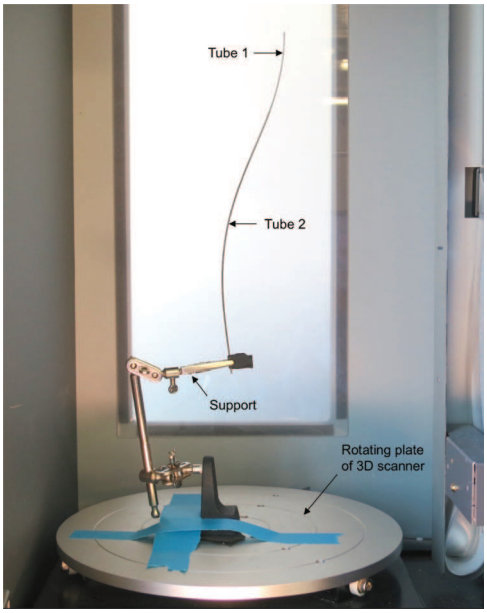

Fig. 14. Experimental set-up with device held vertically inside 3D laser scanner.

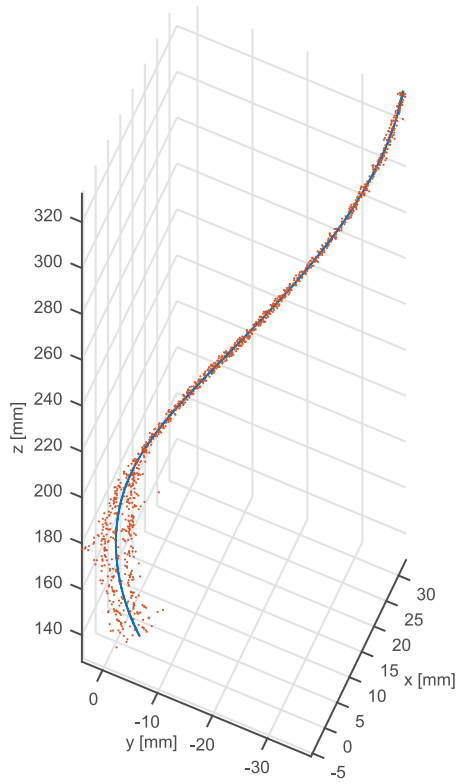

Fig. 15. Exemplary measurement of the 3D device geometry as a cloud of orange points, with a fitted 3D curve in blue.

This rotational behavior is necessary in this configuration, corresponding to follow-the-leader, where the curvature at each point in the workspace must be constant. For tubes with constant stiffness, as in this experiment, follow-the-leader requires the curvature vector of each tube to remain constant at each point in the workspace. Since the tubes are in a minimum energy equilibrium at the beginning of the experiment, tube 1 is expected to rotate to remain in the minimum energy equilibrium as it is being inserted. Considering that the tubes have a helical geometry, remaining at a minimum energy configuration implies maintaining a constant-curvature vector at each point in the workspace, and therefore rotating at the follow-the-leader rate w_1. This structural behavior can therefore be exploited to design a simpler experiment that suffices to illustrate the research on follow-the-leader, which is the strategy adopted in this work for the implementation.

The experimental set-up used in the implementation is shown in Figure 14. The shape of the device is measured at regular intervals during advancement using a 3D laser scanner (PICZA LPX-250, manufactured by Roland). The desired initial geometry of the tubes was achieved by means of a shape-setting process. Since the tubes' stiffness is constant, their precurvatures are helical, and the shape-setting process simply involved constraining each tube to a cylindrical fixture of the specified diameter, heating the assembly in air to 550 °C under free convection for 10 min, and quenching it in water. The assembled device with both tubes arranged concentrically was held vertically to minimize deformation due to gravitational forces. In this work, the set-up was placed inside the 3D laser scanner, and tube 1 was advanced manually while tube 2 remained fixed relative to the scanner workspace.

Six robot shape measurements were recorded using the 3D laser scanner as tube 1 was advanced. Each measurement consists of a set of points describing the device shape, as shown in Figure 15 for the third measurement, with the corresponding projections on the XZ and YZ planes, shown in Figures 16 and 17, respectively. A curve is fitted to determine the geometry of the curve corresponding to the device centerline, which is also shown in Figures 15 to 17, for the same measurement. As can be seen, the measurement presents a certain degree of noise, which is mainly caused by the vibrations induced in the device by the rotation of the 3D scanner. The noise is zero mean, and the fitted curve allows for reliable extraction of the geometry of the device. The fitted curves of the different measurements are subsequently used to assess the follow-the-leader motion.

The result of the experiment is an accurate follow-the-leader configuration throughout the entire device. The 3D points from the different measurements recorded during device advancement, together with their corresponding fitted curves, are shown in Figure 18, using specific colors for each measurement. The projections of the fitted curves on the XZ and YZ planes are shown in Figures 19 and 20, respectively. As can be seen, the motion in both parts of the trajectory, corresponding to two tubes and one tube, remains within a follow-the-leader configuration. The maximum deviation estimated from the fitted curves in each measurement is 4 mm. This can be partially attributed to

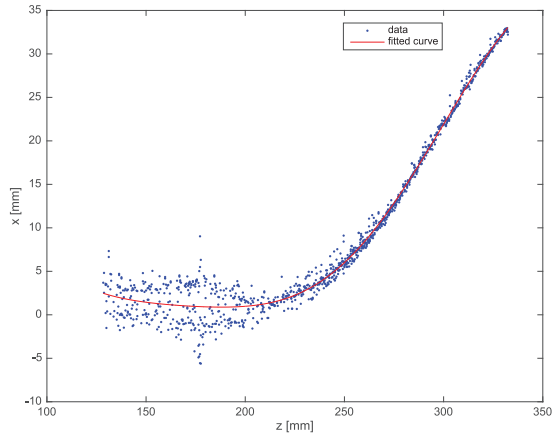

Fig. 16. Projection on the XZ plane of the recorded points describing the geometry of the device in one exemplary measurement, with the corresponding fitted curve.

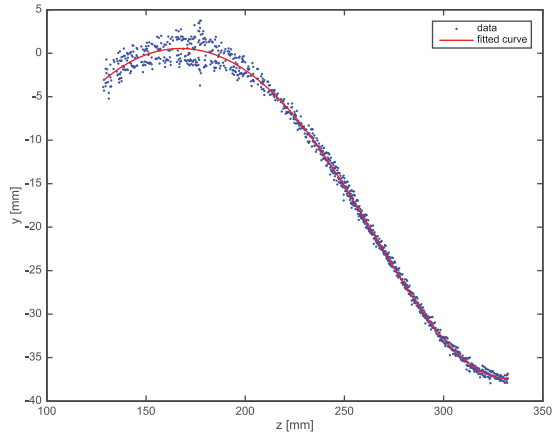

Fig. 17. Projection on the YZ plane of the measured points corresponding to the device shape in a specific configuration during the experiment, and fitted curve.

the limited accuracy of the experimental set-up, 3D scanner, and shape-setting process, as well as small discrepancies between the idealized robot behavior and the practical implementation, mainly in terms of external forces or friction between the tubes.

The trajectory displayed by the device in the experiment presents the same approximate characteristics as the planned trajectory, as shown in Figure 21, although there are some discrepancies. The discrepancies are considered to be related to imperfections in the experimental implementation, as well as small inaccuracies in the assumptions used in the derivation. Interestingly, in the experimental implementation, tube 1 presented an estimated rotation at the expected rate as it was being inserted, according to visual observation of the rotation at the base of the tube aided by markers. The apparent torsion of the tubes, also estimated from visual observations at $\alpha(0)$ and $\alpha(L - h_2)$ aided by markers, was minimal, as predicted. Overall, and despite

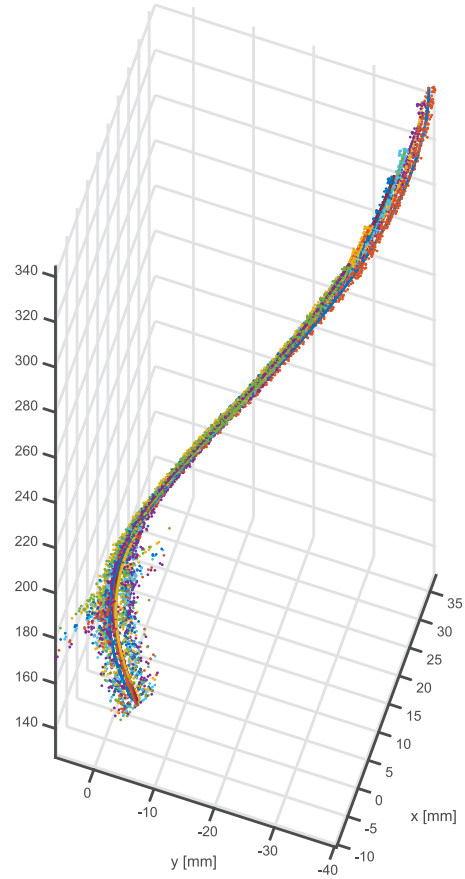

Fig. 18. Experimental measurements of the device geometry during the advancement of one of the tubes, plotted as a point cloud with a different color for each recorded configuration. The different measurements overlap, confirming follow-the-leader motion throughout the entire device. The curves fitted to each measurement are also displayed.

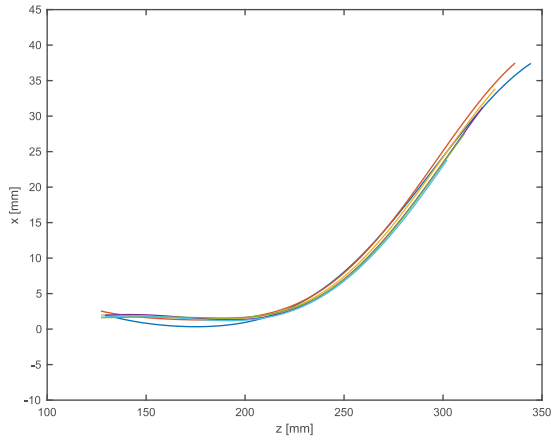

Fig. 19. Projection on the XZ plane of the curves fitted to the experimental measurements during advancement of one of the tubes.

practical imperfections, the experiment satisfactorily illustrates the research on follow-the-leader kinematics and on torsion of the tubes.

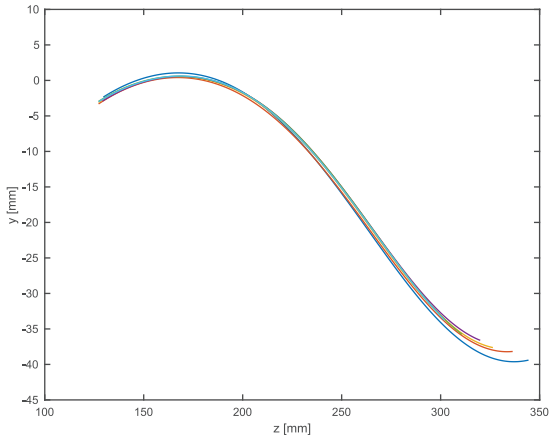

Fig. 20. Projection on the YZ plane of the curves fitted to the experimental measurements during advancement of one of the tubes.

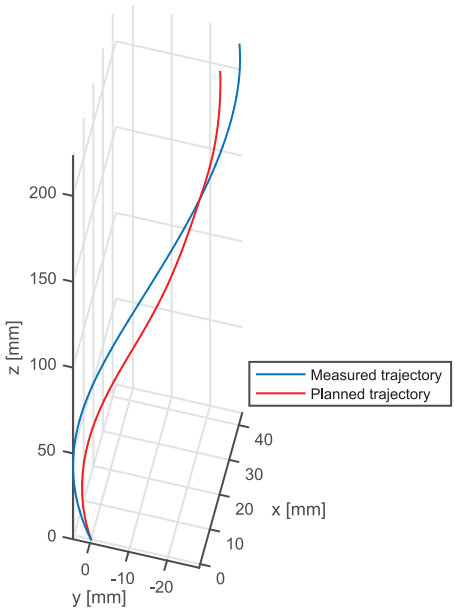

Fig. 21. Planned and measured trajectories.

7. Conclusions

Follow-the-leader motion using concentric tube robots is possible in a broader set of trajectories than those currently being exploited. The complete set of trajectories where follow-the-leader motion is possible under the assumption of no axial torsion within the robot was derived in this work, yielding a closed-form solution. The solution obtained showed that the majority of trajectories in the set present a continuous variation of curvature along the arc length, in both direction and magnitude; still, the solution includes all currently known piecewise constant-curvature trajectories as a particular case. The analysis presented in this paper also elucidated the control required for a robot to advance in a follow-the-leader configuration, where the individual tubes must either be static or advancing as part of the robot's distal end. Furthermore, additional maneuvers of interest were extracted from the study of follow-the-leader kinematics. These include the possibility of combining follow-the-leader motion in the proximal part of the robot with general motion at the distal end, or the linkage of trajectories that can be traced in follow-the-leader configuration. The general analysis of follow-the-leader motion was developed under the assumption of no axial torsion of the tubes. To determine the validity of such an assumption, and then select a stable robot configuration to showcase follow-the-leader motion in practice, the torsion of the tubes was considered in the trajectories of interest. A closed-form solution describing the torsion of the tubes in the most relevant trajectories where follow-the-leader is possible using two-tube robots was derived. Criteria for the structural stability of the robot were then extracted from such a solution, and a relevant subset of designs was explored. This allowed for the identification of stable trajectories that can be traced in follow-the-leader motion within an admissible deviation value, which can be specified as desired. A suitable stable trajectory was selected as a case study of a prototypical, two-tube concentric tube robot. The case study was developed with simulations and an experiment, showcasing the capability of follow-the-leader motion in a trajectory with continuous curvature variation, in both direction and magnitude. This capability in the wider set of trajectories found in this work expands the potential of concentric tube robots in minimally invasive surgery, offering the possibility for new or improved procedures.

Funding

The author(s) disclosed receipt of the following financial support for the research, authorship, and/or publication of this article: This work was supported by the Engineering and Physical Sciences Research Council [grant number EP/L015587/1], and Rolls-Royce plc.

References

Bergeles C and Dupont PE (2013) Planning stable paths for concentric tube robots. In: *2013 IEEE international conference on intelligent robots and systems (IROS)*, Tokyo, Japan, 3–7 November 2013, pp. 3077–3082. Piscataway, NJ: IEEE.

Bishop RL (1975) There is more than one way to frame a curve. *American Mathematical Monthly* 82: 246–251.

Burgner J, Swaney PJ, Rucker DC, et al. (2011) A bimanual teleoperated system for endonasal skull base surgery. In: *2011 IEEE/RSJ international conference on intelligent robots and systems*, San Francisco, CA, 25–30 September 2011, pp. 2517–2523. Piscataway, NJ: IEEE.

Butler EJ, Hammond-Oakley R, Chawarski S, et al. (2012) Robotic neuro-endoscope with concentric tube augmentation. In: *2012 IEEE international conference on intelligent robots and systems (IROS)*, Vilamoura, Portugal, 7–12 October 2012, pp. 2941–2946. Piscataway, NJ: IEEE.

Dupont PE, Gosline A, Vasilyev N, et al. (2012) Concentric tube robots for minimally invasive surgery. In: *Hamlyn symposium*

on medical robotics, London, UK, 1–2 July 2012, pp. 3–5. London: The Hamlyn Centre.

Dupont PE, Lock J, and Butler E (2009) Torsional kinematic model for concentric-tube robots. In: *2009 IEEE international conference on robotics and automation (ICRA)*, Kobe, Japan, 12–17 May 2009, pp. 3851–3858. Piscataway, NJ: IEEE.

Dupont PE, Lock J, and Itkowitz B (2010a) Real-time position control of concentric tube robots. In: *2010 IEEE international conference on robotics and automation (ICRA)*, Anchorage, AK, 3–8 May 2010, pp. 562–568. Piscataway, NJ: IEEE.

Dupont PE, Lock J, Itkowitz B, et al. (2010b) Design and control of concentric-tube robots. *IEEE Transactions on Robotics* 26(2): 209–225.

Gilbert HB, Neimat J, and Webster RJ III (2015) Concentric tube robots as steerable needles: Achieving follow-the-leader deployment. *IEEE Transactions on Robotics* 31(2): 246–258.

Gosline AH, Vasilyev NV, Butler EJ, et al. (2012) Percutaneous intracardiac beating-heart surgery using metal MEMS tissue. *International Journal of Robotics Research* 31(9): 1081–1093.

Greenblatt E, Trovato T, Popovic A, et al. (2011) *Interlocking nested cannula*. Patent US20110201887A1, USA.

Lock J and Dupont PE (2011) Friction modeling in concentric tube robots. In: *2011 IEEE international conference on robotics and automation (ICRA)*, Shanghai, China, 9–13 May 2011, pp. 1139–1146. Piscataway, NJ: IEEE.

Lyons LA, Webster RJ III, and Alterovitz R (2009) Motion planning for active cannulas. In: *2009 IEEE/RSJ international conference on intelligent robots and systems (IROS)*, St. Louis, MO, 11–15 October 2009, pp. 801–806. Piscataway, NJ: IEEE.

Lyons LA, Webster RJ III, and Alterovitz R (2010) Planning active cannula configurations through tubular anatomy. In: *2010 IEEE international conference on robotics and automation*, Anchorage, AK, 3–8 May 2010, pp. 2082–2087. Piscataway, NJ: IEEE.

Mahvash M and Dupont PE (2011) Stiffness control of surgical continuum manipulators. *IEEE Transactions on Robotics* 27(2): 334–345.

Rucker DC, Jones BA, and Webster RJ III (2010) A geometrically exact model for externally loaded concentric-tube continuum robots. *IEEE Transactions on Robotics* 26(5): 769–780.

Ryu SC and Dupont PE (2014) FBG-based shape sensing tubes for continuum robots. In: *2014 IEEE international conference on robotics and automation*, Hong Kong, 31 May–7 June 2014, pp. 3531–3537. Piscataway, NJ: IEEE.

Sears P and Dupont PE (2006) A steerable needle technology using curved concentric tubes. In: *2006 IEEE/RSJ international conference on intelligent robots and systems*, Beijing, China, 9–15 October 2006, pp. 2850–2856. Piscataway, NJ: IEEE.

Vasilyev NV, Gosline AH, Butler E, et al. (2013) Percutaneous steerable robotic tool delivery platform and metal microelectromechanical systems device for tissue manipulation and approximation: Closure of patent foramen ovale in an animal model. *Circulation: Cardiovascular Interventions* 6: 468–475.

Webster RJ III, Okamura AM, and Cowan NJ (2006) Toward active cannulas: Miniature snake-like surgical robots. In: *2006 IEEE international conference on intelligent robots and systems (IROS)*, Beijing, China, 9–15 October 2006, pp. 2857–2863.

Webster RJ III, Romano JM, and Cowan NJ (2009) Mechanics of precurved-tube continuum robots. *IEEE Transactions on Robotics* 25(1): 67–78.

Appendix A

The derivation of equation (32) is described here. Recalling the definition of u_{iz} as the torsional strain, the derivative of equation (31) with respect to the arc length relates the twist rate to the torsion of the tubes

$$\dot{\alpha} = u_{2z} - u_{1z} \tag{43}$$

Combining the equilibrium of moments (equation (2)) in the z direction and the constitutive law (equation (1)), the following relation in the z direction can be obtained

$$k_{1z}u_{1z} + k_{2z}u_{2z} = 0 \tag{44}$$

Substituting equation (44) into equation (43), the twist rate between both tubes can be related to the torsion of one of the tubes

$$\dot{\alpha} = \left(1 + \frac{k_{2z}}{k_{1z}}\right) u_{2z} \tag{45}$$

It should be noted that the twist rate can also be directly related to the torsion of the other tube using equation (44).

Finally, the derivative of equation (45) can be combined with equation (30), yielding

$$\ddot{\alpha} = \left(\frac{k_{2x}}{k_{2z}} + \frac{k_{2x}}{k_{1z}}\right)\left(u_{2x}\hat{u}_{2y} - u_{2y}\hat{u}_{2x}\right) \tag{46}$$

Appendix B

The derivation of the solution to equation (39) with boundary conditions (equation (40)), and its application to solve equation (37), are described in the following.

The approach adopted in this work relies on the fact that equation (39) is analogous to the equation of a non-linear pendulum. Thus, the solution to a non-linear pendulum is adapted here for the specific boundary conditions (equation (40)). Considering that

$$\frac{\mathrm{d}^2 f(\zeta)}{\mathrm{d}\zeta^2} = \ddot{f} = \dot{f}\frac{\mathrm{d}\dot{f}}{\mathrm{d}f}$$

equation (39) can be integrated

$$\int_{\dot{f}(0)}^{\dot{f}(\zeta)} \dot{f}\,\mathrm{d}\dot{f} = c\int_{f(0)}^{f(\zeta)} \sin(f)\,\mathrm{d}f \tag{47}$$

and evaluated as

$$\dot{f}(\zeta)^2 = \dot{f}(0)^2 + 2c(\cos(f(0)) - \cos(f(\zeta))) \tag{48}$$

This expression can be evaluated at $\zeta = L$, considering the boundary conditions (equation (40)), and substituted in equation (48), resulting in

$$\dot{f}(\zeta)^2 = (w_2 - w_1)^2 + 2c(\cos(f(L)) - \cos(f(\zeta))) \tag{49}$$

Using separation of variables, the integral of equation (49) can be considered in the following interval

$$\zeta - L = \frac{1}{\sqrt{2c}}\int_{f(L)}^{f(\zeta)} \frac{\mathrm{d}f}{\sqrt{\frac{(w_2-w_1)^2}{2c} + \cos(f(L)) - \cos(f(\zeta))}} \tag{50}$$

Considering the variable definitions

$$b = \frac{(w_2 - w_1)^2}{2c} + \cos(f(L)) + 1$$

$K_e = \sqrt{(2/b)}$, and using the change of variable $h(\zeta) = f(\zeta) + \pi$, equation (50) can be rewritten as

$$\zeta - L = \frac{1}{\sqrt{2cb}} \int_{h(L)}^{h(\zeta)} \frac{\mathrm{d}h}{\sqrt{1 - {K_e}^2 \sin^2 \frac{h(\zeta)}{2}}} \tag{51}$$

This integral corresponds to the incomplete elliptic integral of the first kind $F(x, K)$, which is defined for $0 \leq K \leq 1$. The closed-form solution to equation (51) can be obtained in two intervals of K_e.

If $0 \leq K_e \leq 1$, equation (51) can be directly integrated according to the definition of $F(x, K)$, yielding

$$(\zeta - L)\sqrt{\frac{cb}{2}} = F\left(\frac{h(\zeta)}{2}, K_e\right) - F\left(\frac{h(L)}{2}, K_e\right) \tag{52}$$

Using the Jacobi elliptic functions *sn* and *cn*, the incomplete elliptic integral of the first kind

$$F\left(\frac{h(\zeta)}{2}, K_e\right)$$

can be inverted, which allows one to solve for $h(\zeta)$ as

$$h(\zeta) = 2\tan^{-1}\left[\frac{sn\left((\zeta - L)\sqrt{\frac{cb}{2}} + F\left(\frac{h(L)}{2}, K_e\right), K_e\right)}{cn\left((\zeta - L)\sqrt{\frac{cb}{2}} + F\left(\frac{h(L)}{2}, K_e\right), K_e\right)}\right] \tag{53}$$

If $K_e > 1$, a change of variable can be defined using

$$\psi(\zeta) = \sin^{-1}\left(K_e \sin\frac{h(\zeta)}{2}\right) \tag{54}$$

which can be differentiated as

$$\mathrm{d}\psi \cos\psi = K_e \sqrt{1 - \frac{\sin^2\psi}{{K_e}^2}} \frac{\mathrm{d}h}{2} \tag{55}$$

and guarantees that the incomplete elliptic integral is well defined. Applying such a change of variable to equation (51) yields

$$(\zeta - L)\sqrt{c} = \int_{\psi(L)}^{\psi(\zeta)} \frac{\cos\psi \,\mathrm{d}\psi}{\sqrt{1 - \frac{\sin^2\psi}{{K_e}^2}}\sqrt{1 - \sin^2\psi}} \tag{56}$$

which can be integrated using the definition of the incomplete integral of the first kind, resulting in

$$(\zeta - L)\sqrt{c} = F\left(\psi(\zeta), \frac{1}{K_e}\right) - F\left(\psi(L), \frac{1}{K_e}\right) \tag{57}$$

Using Jacobi elliptic functions, and reversing the change of variables, equation (57) can be solved for $h(\zeta)$ as

$$h(\zeta) = 2\sin^{-1}\left\{\frac{1}{K_e} sn\left[(\zeta - L)\sqrt{c} + F\left(\sin^{-1}\left[K_e \sin\left(\frac{h(L)}{2}\right)\right], \frac{1}{K_e}\right), \frac{1}{K_e}\right]\right\} \tag{58}$$

The change of variable $h(\zeta) = f(\zeta) + \pi$ can be reversed to obtain the solution to equation (39) from equations (53) and (58), which is immediate. Finally, reversing the change of variable (equation (38)), the solution to equation (37) can be obtained for $0 \leq K_e \leq 1$ as

$$\alpha(\zeta) = (w_1 - w_2)\zeta - \pi - \phi_d + 2\tan^{-1}\left[\frac{sn\left((\zeta - L)\sqrt{\frac{cb}{2}} + F\left(\frac{\alpha(L) + (w_2 - w_1)L + \phi_d + \pi}{2}, K_e\right), K_e\right)}{cn\left((\zeta - L)\sqrt{\frac{cb}{2}} + F\left(\frac{\alpha(L) + (w_2 - w_1)L + \phi_d + \pi}{2}, K_e\right), K_e\right)}\right] \tag{59}$$

and for $K_e > 1$ as

$$\alpha(\zeta) = (w_1 - w_2)\zeta - \pi - \phi_d + 2\sin^{-1}\left\{\frac{1}{K_e} sn\left[(\zeta - L)\sqrt{c} + F\left(\sin^{-1}\left[K_e \sin\left(\frac{\alpha(L) + (w_2 - w_1)L + \phi_d + \pi}{2}\right)\right], \frac{1}{K_e}\right), \frac{1}{K_e}\right]\right\} \tag{60}$$